



**HAL**  
open science

## A study of strange particle production in $\nu_\mu$ charged current interactions in the NOMAD experiment

P. Astier, D. Autiero, A. Baldisseri, M. Baldo-Ceolin, M. Banner, G. Bassompierre, N. Besson, I. Bird, B. Blumenfeld, F. Bobisut, et al.

### ► To cite this version:

P. Astier, D. Autiero, A. Baldisseri, M. Baldo-Ceolin, M. Banner, et al.. A study of strange particle production in  $\nu_\mu$  charged current interactions in the NOMAD experiment. Nuclear Physics B, 2002, 621, pp.3-34. in2p3-00013597

**HAL Id: in2p3-00013597**

**<https://in2p3.hal.science/in2p3-00013597v1>**

Submitted on 12 Mar 2002

**HAL** is a multi-disciplinary open access archive for the deposit and dissemination of scientific research documents, whether they are published or not. The documents may come from teaching and research institutions in France or abroad, or from public or private research centers.

L'archive ouverte pluridisciplinaire **HAL**, est destinée au dépôt et à la diffusion de documents scientifiques de niveau recherche, publiés ou non, émanant des établissements d'enseignement et de recherche français ou étrangers, des laboratoires publics ou privés.

## A STUDY OF STRANGE PARTICLE PRODUCTION IN $\nu_\mu$ CHARGED CURRENT INTERACTIONS IN THE NOMAD EXPERIMENT

### NOMAD Collaboration

P. Astier<sup>1)</sup> D. Autiero<sup>2)</sup> A. Baldisseri<sup>3)</sup> M. Baldo-Ceolin<sup>4)</sup> M. Banner<sup>1)</sup> G. Bassompierre<sup>5)</sup>  
 K. Benslama<sup>6)</sup> N. Besson<sup>3)</sup> I. Bird<sup>2,6)</sup> B. Blumenfeld<sup>7)</sup> F. Bobisut<sup>4)</sup> J. Bouchez<sup>3)</sup> S. Boyd<sup>8)</sup>  
 A. Bueno<sup>9,10)</sup> S. Bunyatov<sup>11)</sup> L. Camilleri<sup>2)</sup> A. Cardini<sup>12)</sup> P.W. Cattaneo<sup>13)</sup> V. Cavasinni<sup>14)</sup>  
 A. Cervera-Villanueva<sup>2,15)</sup> R. Challis<sup>20)</sup> A. Chukanov<sup>11)</sup> G. Collazuol<sup>4)</sup> G. Conforto<sup>2,16)</sup>  
 C. Conta<sup>13)</sup> M. Contalbrigo<sup>4)</sup> R. Cousins<sup>12)</sup> D. Daniels<sup>9)</sup> H. Degaudenzi<sup>6)</sup> T. Del Prete<sup>14)</sup>  
 A. De Santo<sup>2)</sup> T. Dignan<sup>9)</sup> L. Di Lella<sup>2)</sup> E. do Couto e Silva<sup>2)</sup> J. Dumarchez<sup>1)</sup> M. Ellis<sup>8)</sup>  
 T. Fazio<sup>5)</sup> G.J. Feldman<sup>9)</sup> R. Ferrari<sup>13)</sup> D. Ferrère<sup>2)</sup> V. Flaminio<sup>14)</sup> M. Fraternali<sup>13)</sup>  
 J.-M. Gaillard<sup>5)</sup> E. Gangler<sup>2,1)</sup> A. Geiser<sup>17,2)</sup> D. Geppert<sup>17)</sup> D. Gibin<sup>4)</sup> S. Gninenko<sup>2,18)</sup>  
 A. Godley<sup>23,8)</sup> J.-J. Gomez-Cadenas<sup>2,15)</sup> J. Gosset<sup>3)</sup> C. Gößling<sup>17)</sup> M. Gouanère<sup>5)</sup> A. Grant<sup>2)</sup>  
 G. Graziani<sup>19)</sup> A. Guglielmi<sup>4)</sup> C. Hagner<sup>3)</sup> J. Hernando<sup>15)</sup> D. Hubbard<sup>9)</sup> P. Hurst<sup>9)</sup> N. Hyett<sup>20)</sup>  
 E. Iacopini<sup>19)</sup> C. Joseph<sup>6)</sup> F. Juliet<sup>6)</sup> N. Kent<sup>20)</sup> M. Kirsanov<sup>18)</sup> O. Klimov<sup>11)</sup> J. Kokkonen<sup>2)</sup>  
 A. Kovzelev<sup>18,13)</sup> A. Krasnoperov<sup>5,11)</sup> D. Kustov<sup>11)</sup> V. Kuznetsov<sup>11,2)</sup> S. Lacaprara<sup>4)</sup>  
 C. Lachaud<sup>1)</sup> B. Lakić<sup>21)</sup> A. Lanza<sup>13)</sup> L. La Rotonda<sup>22)</sup> M. Laveder<sup>4)</sup> A. Letessier-Selvon<sup>1)</sup>  
 J.-M. Levy<sup>1)</sup> L. Linssen<sup>2)</sup> A. Ljubičić<sup>21)</sup> J. Long<sup>7)</sup> A. Lupi<sup>19)</sup> A. Marchionni<sup>19)</sup> F. Martelli<sup>16)</sup>  
 X. Méchain<sup>3)</sup> J.-P. Mendiburu<sup>5)</sup> J.-P. Meyer<sup>3)</sup> M. Mezzetto<sup>4)</sup> S.R. Mishra<sup>9,23)</sup>  
 G.F. Moorhead<sup>20)</sup> D. Naumov<sup>11)</sup> P. Nédélec<sup>5)</sup> Yu. Nefedov<sup>11)</sup> C. Nguyen-Mau<sup>6)</sup> D. Orestano<sup>24)</sup>  
 F. Pastore<sup>24)</sup> L.S. Peak<sup>8)</sup> E. Pennacchio<sup>16)</sup> H. Pessard<sup>5)</sup> R. Petti<sup>2,13)</sup> A. Placci<sup>2)</sup> G. Polesello<sup>13)</sup>  
 D. Pollmann<sup>17)</sup> A. Polyarush<sup>18)</sup> B. Popov<sup>11,1)</sup> C. Poulsen<sup>20)</sup> J. Rico<sup>10)</sup> P. Riemann<sup>17)</sup>  
 C. Roda<sup>2,14)</sup> A. Rubbia<sup>2,10)</sup> F. Salvatore<sup>13)</sup> K. Schahmanche<sup>1)</sup> B. Schmidt<sup>17,2)</sup> T. Schmidt<sup>17)</sup>  
 M. Seviar<sup>20)</sup> D. Sillou<sup>5)</sup> F.J.P. Soler<sup>2,8)</sup> G. Sozzi<sup>6)</sup> D. Steele<sup>7,6)</sup> U. Stiegler<sup>2)</sup> M. Stipčević<sup>21)</sup>  
 Th. Stolarczyk<sup>3)</sup> M. Tareb-Reyes<sup>6)</sup> G.N. Taylor<sup>20)</sup> V. Tereshchenko<sup>11)</sup> A. Toropin<sup>18)</sup>  
 A.-M. Touchard<sup>1)</sup> S.N. Tovey<sup>2,20)</sup> M.-T. Tran<sup>6)</sup> E. Tsemelis<sup>2)</sup> J. Ulrichs<sup>8)</sup> L. Vacavant<sup>6)</sup>  
 M. Valdata-Nappi<sup>22,\*)</sup> V. Valuev<sup>11,12)</sup> F. Vannucci<sup>1)</sup> K.E. Varvell<sup>8)</sup> M. Veltri<sup>16)</sup> V. Vercesi<sup>13)</sup>  
 G. Vidal-Sitjes<sup>2)</sup> J.-M. Vieira<sup>6)</sup> T. Vinogradova<sup>12)</sup> F.V. Weber<sup>9,2)</sup> T. Weisse<sup>17)</sup> F.F. Wilson<sup>2)</sup>  
 L.J. Winton<sup>20)</sup> B.D. Yabsley<sup>8)</sup> H. Zacccone<sup>3)</sup> K. Zuber<sup>17)</sup> P. Zuccon<sup>4)</sup>

### ABSTRACT

A study of strange particle production in  $\nu_\mu$  charged current interactions has been performed using the data from the NOMAD experiment. Yields of neutral strange particles ( $K_s^0$ ,  $\Lambda$ ,  $\bar{\Lambda}$ ) have been measured. Mean multiplicities are reported as a function of the event kinematic variables  $E_\nu$ ,  $W^2$  and  $Q^2$  as well as of the variables describing particle behaviour within a hadronic jet:  $x_F$ ,  $z$  and  $p_T^2$ . Decays of resonances and heavy hyperons with identified  $K_s^0$  and  $\Lambda$  in the final state have been analyzed. Clear signals corresponding to  $K^{*\pm}$ ,  $\Sigma^{*\pm}$ ,  $\Xi^-$  and  $\Sigma^0$  have been observed.

*(To be published in Nuclear Physics B)*

- 
- 1) LPNHE, Univ. of Paris VI and VII, Paris, France
  - 2) CERN, Geneva, Switzerland
  - 3) DAPNIA, CEA Saclay, France
  - 4) Univ. of Padova and INFN, Padova, Italy
  - 5) LAPP, Annecy, France
  - 6) University of Lausanne, Lausanne, Switzerland
  - 7) Johns Hopkins Univ., Baltimore, MD, USA
  - 8) Univ. of Sydney, Sydney, Australia
  - 9) Harvard Univ., Cambridge, MA, USA
  - 10) ETH Zürich, Zürich, Switzerland
  - 11) JINR, Dubna, Russia
  - 12) UCLA, Los Angeles, CA, USA
  - 13) Univ. of Pavia and INFN, Pavia, Italy
  - 14) Univ. of Pisa and INFN, Pisa, Italy
  - 15) IFIC, Valencia, Spain
  - 16) Univ. of Urbino, Urbino, and INFN Florence, Italy
  - 17) Dortmund Univ., Dortmund, Germany
  - 18) Inst. Nucl. Research, INR Moscow, Russia
  - 19) Univ. of Florence and INFN, Florence, Italy
  - 20) University of Melbourne, Melbourne, Australia
  - 21) Rudjer Bošković Institute, Zagreb, Croatia
  - 22) Univ. of Calabria and INFN, Cosenza, Italy
  - 23) Univ. of South Carolina, Columbia, SC, USA
  - 24) Roma Tre University and INFN, Rome, Italy
  - \*) Now at Univ. of Perugia and INFN, Perugia, Italy

# 1 INTRODUCTION

The production of strange particles in neutrino interactions can provide a testing ground for the quark-parton as well as for hadronization models. Neutral strange particles can be reliably identified using the  $V^0$ -like signature of their decays ( $K_s^0 \rightarrow \pi^+\pi^-$ ,  $\Lambda \rightarrow p\pi^-$  and  $\bar{\Lambda} \rightarrow \bar{p}\pi^+$ ) in contrast to most other hadrons which require particle identification hardware. It is noteworthy that all previous investigations of strange particle production by neutrinos have come from bubble chamber experiments [1, 2, 3, 4, 5, 6, 7, 8, 9, 10, 11, 12, 13, 14, 15, 16, 17, 18, 19, 20, 21, 22, 23, 24, 25]. No other technique has so far yielded results on this subject. However, previous bubble chamber experiments with (anti)neutrino beams suffered from the low statistics of their  $V^0$  samples.

The NOMAD experiment [26] has collected a large number of neutrino interactions with a reconstruction quality similar to that of bubble chamber experiments. The order of magnitude increase in statistics can be used to improve our knowledge of strange particle production in neutrino interactions. In this paper we present measurements of the yields of neutral strange particles ( $K_s^0$ ,  $\Lambda$  and  $\bar{\Lambda}$ ), as well as the yields of  $K^{*\pm}$ ,  $\Sigma^{*\pm}$ ,  $\Xi^-$  and  $\Sigma^0$  in  $\nu_\mu$  charged current (CC) interactions. These results are compared to the predictions of the NOMAD Monte Carlo (MC) simulation program.

The results of the present analysis are the measurements of:

1. the production properties of neutral strange particles in  $\nu_\mu$  CC interactions. This study will allow tuning of the parameters of the MC simulation programs in order to correctly reproduce the production of strange particles by neutrinos;
2. the contribution of strange resonances and heavy hyperons to the total number of observed  $K_s^0$ ,  $\Lambda$  and  $\bar{\Lambda}$ . This will allow a quantitative theoretical interpretation of the  $\Lambda$  and  $\bar{\Lambda}$  polarization measurements in  $\nu_\mu$  CC deep inelastic scattering (DIS) reported in our previous articles [27, 28].

## 2 EXPERIMENTAL PROCEDURE

### 2.1 The NOMAD experiment

The main goal of the NOMAD experiment [26] was the search for  $\nu_\mu \rightarrow \nu_\tau$  oscillations in a wide-band neutrino beam from the CERN SPS. The main characteristics of the beam are given in Table 1. This search uses kinematic criteria to identify  $\nu_\tau$  CC interactions [29] and requires a very good quality of event reconstruction similar to that of bubble chamber experiments. This has indeed been achieved by the NOMAD detector, and, moreover, the large data sample collected during four years of data taking (1995-1998) allows for a detailed study of neutrino interactions. The full data sample from the NOMAD experiment corresponding to about 1.3 million  $\nu_\mu$  CC interactions in the detector fiducial volume is used in the present analysis. The data are compared to the results of a Monte Carlo simulation based on modified versions of LEPTO 6.1 [30] and JETSET 7.4 [31] generators for neutrino interactions (with  $Q^2$  and  $W^2$  cutoff parameters removed) and on a GEANT [32] based program for the detector response. Strange particle production is described by the set of default parameters in JETSET. To define the parton content of the nucleon for the cross-section calculation we have used the GRV-HO parametrization [33] of the parton density functions available in PDFLIB [34]. The above description of the MC will be referred to as the default MC. For the analysis reported below we used a MC sample consisting of about 3 million events.

Table 1: *The CERN SPS neutrino beam composition at the position of the NOMAD detector (as predicted by the beam simulation program [35]).*

Neutrino flavours	Flux		CC interactions in NOMAD	
	$\langle E_\nu \rangle$ [GeV]	rel.abund.	$\langle E_\nu \rangle$ [GeV]	rel.abund.
$\nu_\mu$	24.2	1	45.3	1
$\bar{\nu}_\mu$	18.5	0.0637	40.9	0.0244
$\nu_e$	36.6	0.0102	57.1	0.0153
$\bar{\nu}_e$	28.7	0.0025	49.9	0.0015

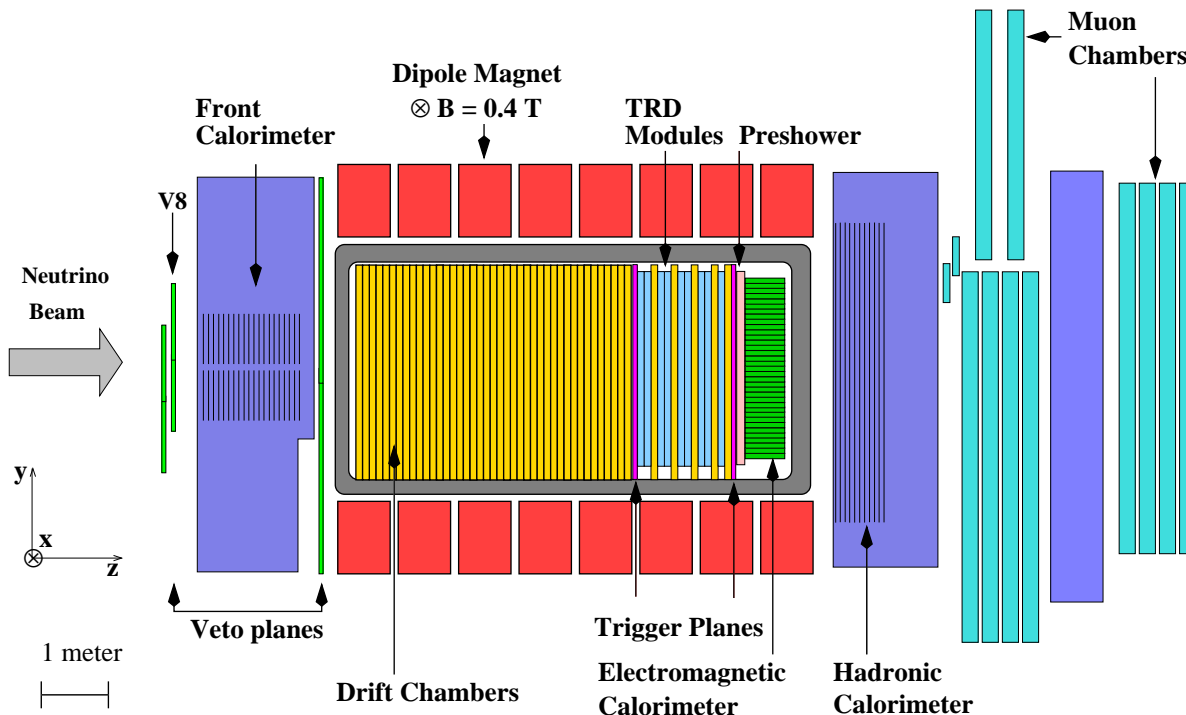


Figure 1: A sideview of the NOMAD detector.

## 2.2 The NOMAD detector

For a study of strange particle production the tracking capabilities of a detector are of paramount importance. The NOMAD detector (Fig. 1) is especially well suited for this. It consists of an active target of 44 drift chambers, with a total fiducial mass of 2.7 tons, located in a 0.4 Tesla dipole magnetic field. The drift chambers (DC) [36], made of low  $Z$  material (mainly carbon) serve the dual role of a nearly isoscalar target for neutrino interactions and of the tracking medium. The average density of the drift chamber volume is  $0.1 \text{ g/cm}^3$ , very close to that of liquid hydrogen. These drift chambers provide an overall efficiency for charged particle reconstruction of better than 95% and a momentum resolution which can be parametrized as

$$\frac{\sigma_p}{p} = \frac{0.05}{\sqrt{L}} \oplus \frac{0.008 \cdot p}{\sqrt{L^5}},$$

where the track length  $L$  is in metres and the track momentum  $p$  is in GeV/c. This amounts to a resolution of approximately 3.5% in the momentum range of interest (less

than 10 GeV/c). Reconstructed tracks are used to determine the event topology (the assignment of tracks to vertices), to reconstruct the vertex position and the track parameters at each vertex and, finally, to identify the vertex type (primary, secondary,  $V^0$ , etc.). A transition radiation detector [37] is used for electron identification. The pion rejection achieved for isolated tracks is  $10^3$  with a 90% electron identification efficiency. A lead-glass electromagnetic calorimeter [38] located downstream of the tracking region provides an energy resolution of  $3.2\%/\sqrt{E[\text{GeV}]} \oplus 1\%$  for electromagnetic showers and is essential to measure the total energy flow in neutrino interactions. In addition, an iron absorber and a set of muon chambers located after the electromagnetic calorimeter are used for muon identification, providing a muon detection efficiency of 97% for momenta greater than 5 GeV/c.

The large statistics of the data combined with the good quality of event reconstruction in the NOMAD detector allows a detailed study of strange particle production in neutrino interactions to be performed.

### 2.3 Event selection and $V^0$ identification procedure

The NOMAD experiment has collected  $1.3 \times 10^6$   $\nu_\mu$  CC events and has observed an unprecedented number of neutral strange particle decays. Such a decay appears in the detector as a  $V^0$ -like vertex: two tracks of opposite charge emerging from a common vertex separated from the primary neutrino interaction vertex (Fig. 2). The  $V^0$ -like signature is expected also for photon conversions.

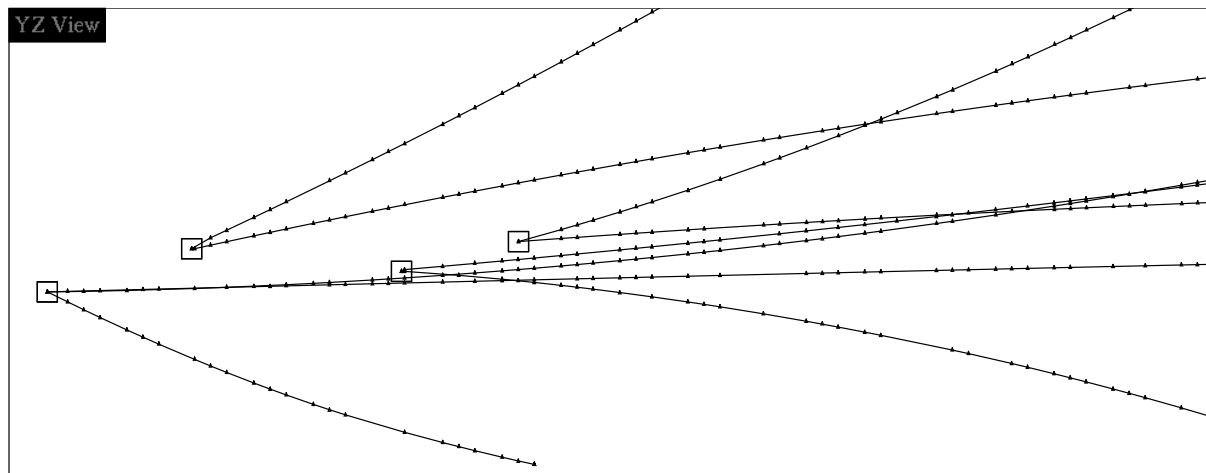


Figure 2: A reconstructed data event containing 3  $V^0$  vertices identified as  $K_s^0$  decays by our identification procedure. The scale on this plot is given by the size of the vertex boxes ( $3 \times 3 \text{ cm}^2$ ).

The selection procedure for the  $\nu_\mu$  CC event sample used in this analysis has been described in [27].

Since the NOMAD detector is unable to distinguish (anti)protons from pions in the momentum range relevant to this analysis, our  $V^0$  identification procedure relies on the kinematic properties of a  $V^0$  decay.

For the  $V^0$  identification a kinematic fit method has been used as described in [27, 39]. This fit has been performed for three decay hypotheses:  $K_s^0 \rightarrow \pi^+\pi^-$ ,  $\Lambda \rightarrow p\pi^-$ ,  $\bar{\Lambda} \rightarrow \bar{p}\pi^+$  and for the hypothesis of a photon conversion to  $e^+e^-$ . The output of the kinematic fits applied to a given  $V^0$  vertex consists of four values of  $\chi_{V^0}^2$  describing the

goodness of these fits. Different regions in the four-dimensional  $\chi^2_{V^0}$  space populated by particles identified as  $K_s^0$ ,  $\Lambda$  and  $\bar{\Lambda}$  have been selected. Identified  $V^0$  are of two types:

- *uniquely* identified  $V^0$ , which, in the four-dimensional  $\chi^2_{V^0}$  space described above, populate regions in which decays of only a single particle type are present;
- *ambiguously* identified  $V^0$ , which populate regions in which decays of different particle types are present.

The treatment of ambiguities aims at selecting a given  $V^0$  decay with the highest efficiency and the lowest background contamination from other  $V^0$  types. An optimum compromise between high statistics of the identified  $V^0$  sample and well understood background contamination is the aim of our identification strategy. The MC simulation program has been used to define the criteria for the kinematic  $V^0$  selection and to determine the purity of the final  $K_s^0$ ,  $\Lambda$  and  $\bar{\Lambda}$  samples. We selected a sample consisting of more than 90% of uniquely identified  $V^0$ . Results are reported in Table 2.

Table 2: *Efficiency ( $\epsilon$ ) and purity ( $P$ ) for each selected  $V^0$  category. Numbers of identified neutral strange particles in the data are also shown in the last column.*

$V^0$	$\epsilon$ (%)	$P$ (%)	Data
$K_s^0$	$22.1 \pm 0.1$	$97.2 \pm 0.1$	15074
$\Lambda$	$16.4 \pm 0.1$	$95.9 \pm 0.1$	8087
$\bar{\Lambda}$	$18.6 \pm 0.5$	$89.7 \pm 0.7$	649

The total  $V^0$  sample in our data contains 15074 identified  $K_s^0$ , 8087 identified  $\Lambda$  and 649 identified  $\bar{\Lambda}$  decays, representing significantly larger numbers than in previous (anti)neutrino experiments performed with bubble chambers [1, 2, 3, 4, 5, 6, 7, 8, 9, 10, 11, 12, 13, 14, 15, 16, 17, 18, 19, 20, 21, 22, 23, 24, 25].

Fig. 3 shows the invariant mass and  $c\tau$  distributions for identified  $K_s^0$ ,  $\Lambda$  and  $\bar{\Lambda}$ . The measured mass and the lifetime of identified neutral strange particles are in agreement with the world averages [40]. The corresponding results are given in Tables 3 and 4.

The efficiencies and purities reported in Table 2 are momentum dependent. However, we have checked that they are applicable to the data because the momenta distributions of identified  $V^0$  and of their decay products are identical in the data and MC simulation.

In the rest of this paper we will always present efficiency corrected distributions.

Table 3: *Measured  $V^0$  mass and resolution (in  $MeV/c^2$ ) for both MC and data.*

$V^0$	MC		Data		PDG [40]
	Mass	Resolution	Mass	Resolution	Mass
$K_s^0$	$497.9 \pm 0.1$	$11.0 \pm 0.1$	$497.9 \pm 0.1$	$11.3 \pm 0.1$	$497.672 \pm 0.031$
$\Lambda$	$1115.7 \pm 0.02$	$4.0 \pm 0.03$	$1116.0 \pm 0.05$	$4.45 \pm 0.05$	$1115.683 \pm 0.006$
$\bar{\Lambda}$	$1116.0 \pm 0.1$	$4.1 \pm 0.1$	$1116.3 \pm 0.1$	$4.8 \pm 0.2$	$1115.683 \pm 0.006$

### 3 YIELDS OF NEUTRAL STRANGE PARTICLES

We have studied the production rates of neutral strange particles ( $K_s^0$ ,  $\Lambda$ ,  $\bar{\Lambda}$ ) in  $\nu_\mu$  CC interactions. The particles can be produced at the primary vertex and also from

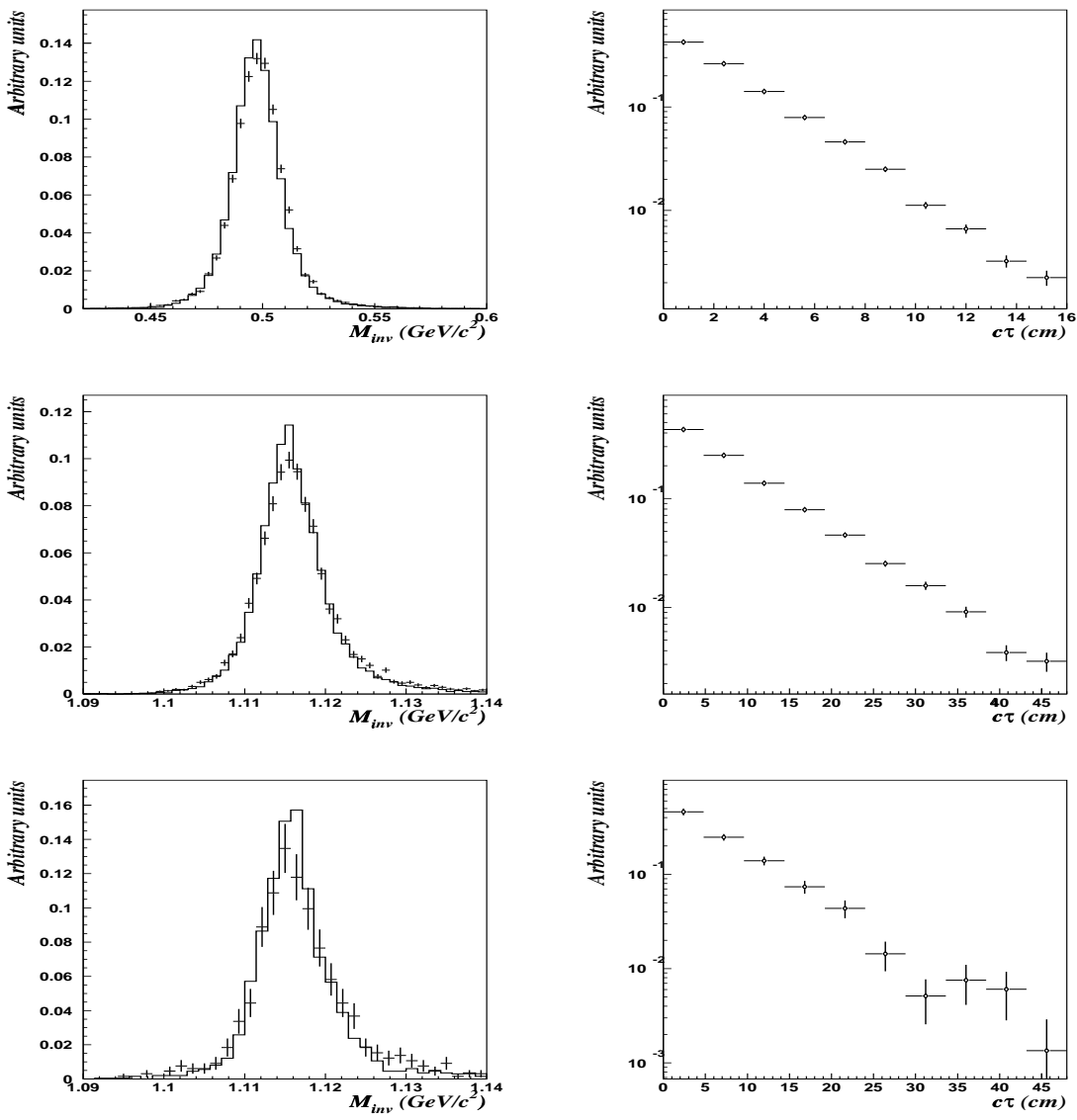


Figure 3: *Invariant mass distributions and efficiency corrected  $c\tau$  distributions for identified  $K_s^0$  (top),  $\Lambda$  (center) and  $\bar{\Lambda}$  (bottom) in  $\nu_\mu$  CC DIS events for both data (points with error bars) and MC (histogram).*

secondary interactions of primary particles with the detector material. Neutral strange particles produced via resonance or heavier hyperon decays are classified as primary  $V^0$ . We applied a correction obtained from the Monte Carlo to the yields of neutral strange particles in the data in order to extract the yields at the primary vertex.

### 3.1 Integral yields of neutral strange particles

The measured yield per  $\nu_\mu$  CC interaction for each  $V^0$  type is defined as:

$$T_{V^0} = \xi \cdot \frac{N_{V^0}}{N_{\nu_\mu \text{CC}}}, \quad (1)$$



Table 4: Measured  $c\tau$  (in cm) for a given  $V^0$  type for both MC and data.

$V^0$	MC	Data	PDG [40]
$K_s^0$	$2.60 \pm 0.01$	$2.72 \pm 0.03$	2.6786
$\Lambda$	$7.91 \pm 0.02$	$8.07 \pm 0.12$	7.89
$\bar{\Lambda}$	$7.82 \pm 0.06$	$7.33 \pm 0.33$	7.89

where  $N_{V^0}$  is the number of reconstructed and identified  $V^0$  in the number  $N_{\nu_\mu CC}$  of reconstructed  $\nu_\mu$  CC events and  $\xi$  is a correction factor calculated as:

$$\xi = \frac{P_{V^0} \times \epsilon_{\nu_\mu CC}}{\epsilon_{V^0} \times Br(V^0 \rightarrow h^+h^-)},$$

where  $\epsilon_{\nu_\mu CC} = (85.30 \pm 0.02)\%$  is the efficiency (reconstruction and identification) of  $\nu_\mu$  CC events in the fiducial volume, and  $\epsilon_{V^0}$  is the global  $V^0$  efficiency which takes into account the contribution from particles produced in the fiducial volume, but decaying outside.  $P_{V^0}$  is the purity of the final  $V^0$  sample, and  $Br(V^0 \rightarrow h^+h^-)$  is the branching ratio for a given  $V^0$  type decaying to a pair of charged hadrons.

Table 5: Integral yields of primary  $V^0$  in  $\nu_\mu$  CC interactions in both the data and in the default MC. The errors are only statistical.

$V^0$ type	$T_{V^0}^{\text{DATA}}$ (%)	$T_{V^0}^{\text{MC}}$ (%)	$T_{V^0}^{\text{MC}}/T_{V^0}^{\text{DATA}}$
$K_s^0$	$6.76 \pm 0.06$	$9.50 \pm 0.02$	$1.40 \pm 0.01$
$\Lambda$	$5.04 \pm 0.06$	$8.10 \pm 0.02$	$1.61 \pm 0.02$
$\bar{\Lambda}$	$0.37 \pm 0.02$	$0.60 \pm 0.01$	$1.62 \pm 0.03$

Table 5 shows the overall inclusive production rates for  $K_s^0$ ,  $\Lambda$  and  $\bar{\Lambda}$  in  $\nu_\mu$  CC interactions compared to the MC predictions. Note that the production rates in the default MC are a factor of 1.4 to 1.6 higher than in the data. This could be explained in part by the choice of the LEPTO [30] and JETSET [31] parameters in the NOMAD event generator. We have to emphasize that the so-called  $s\bar{s}$  suppression factor (PARJ(2) parameter in JETSET) - defined as the ratio of the probability  $\gamma_s$  of producing an  $s\bar{s}$  pair to the probability  $\gamma_u$  ( $\gamma_d$ ) of producing a  $u\bar{u}$  ( $d\bar{d}$ ) pair in the fragmentation chain - was set to its default value of 0.3 in the default NOMAD MC production<sup>1)</sup>. However, this parameter was measured to be about 0.2 in previous bubble chamber experiments: for example, the values obtained by the BEBC WA21 Collaboration [41] in a neutrino beam similar to ours are  $0.200 \pm 0.022(stat) \pm 0.010(sys)$  for  $\bar{\nu}p$  and  $0.207 \pm 0.018(stat) \pm 0.020(sys)$  for  $\nu p$  interactions. Moreover, later results from OPAL (0.245) [42], DELPHI (0.23) [43], E665 (0.2) [44], ZEUS [45] and H1 [46] collaborations support a value close to 0.2 for this parameter.

However, the problem of the inaccurate description of neutral strange particle production in the MC is a more complex one. This is illustrated in Table 6, where we give the observed numbers of  $\nu_\mu$  CC events for 10 exclusive multi- $V^0$  channels in the data

<sup>1)</sup> The value 0.3 has been suggested by the authors of JETSET as the default for this parameter.

Table 6: Numbers of  $\nu_\mu$  CC events with a specified combination of observed neutral strange particle decays for both the default MC and data.  $X$  indicates the hadronic system accompanying the observed  $V^0$ .

Channel	Number of observed events		MC/DATA
	MC	Data	
$\Lambda X$	11686	7778	$1.50 \pm 0.02$
$K_s^0 X$	18971	14228	$1.33 \pm 0.01$
$\bar{\Lambda} X$	831	594	$1.40 \pm 0.07$
$K_s^0 K_s^0 X$	485	284	$1.7 \pm 0.1$
$\Lambda K_s^0 X$	617	247	$2.5 \pm 0.2$
$\Lambda \bar{\Lambda} X$	98	40	$2.5 \pm 0.4$
$K_s^0 \bar{\Lambda} X$	24	15	$1.6 \pm 0.5$
$\Lambda \Lambda X$	19	10	$1.9 \pm 0.7$
$\Lambda K_s^0 K_s^0 X$	7	2	$3.4 \pm 2.6$
$K_s^0 K_s^0 K_s^0 X$	2	4	$0.6 \pm 0.4$

compared to the default MC predictions. The number of MC events in Table 6 is renormalized to the same number of  $\nu_\mu$  CC events as in the data. From this comparison one can conclude that it is not possible to rescale just a single parameter (the  $s\bar{s}$  suppression factor) in order to describe the neutral strange particle production observed in the data. Rather, the discrepancy is due to a combination of several parameters which describe the probability that an  $s(\bar{s})$ -quark appears as a meson/baryon(antibaryon), the probability that a strange meson/baryon(antibaryon) appears electrically neutral, etc. A tuning of the JETSET parameters to reproduce the yields of neutral strange particles observed in the NOMAD data is a subject of an analysis currently in progress.

The integral yields reported in Table 5 can be compared to previous measurements summarized in Table 7. The  $K_s^0$  rates from Table 5 have been converted into  $K^0(= K^0 + \bar{K}^0)$  rates by multiplying by a factor of 2.

For completeness we have recalculated the integral overall yields taking into account contributions from both primary and secondary  $V^0$ . These results are given in Table 7 and denoted by a star ( $\star$ ). Our overall yields are consistent with the results of the  $\nu$ -Ne experiment [19] performed in a similar neutrino beam. However, our primary yields of  $K_s^0$  and  $\Lambda$  are about 30% lower and the primary yield of  $\bar{\Lambda}$  is  $\sim 20\%$  lower.

### 3.2 Yields of neutral strange particles as a function of kinematic variables

To investigate neutral strange particle production mechanisms we have measured the average  $K_s^0$ ,  $\Lambda$  and  $\bar{\Lambda}$  yields as a function of the neutrino energy  $E_\nu$ , the invariant effective mass squared  $W^2$  of the hadronic system, the invariant square of the four-momentum transfer from the neutrino to the target  $Q^2$ , and the Bjorken scaling variable  $x_{Bj}$ .

The yields of  $K_s^0$ ,  $\Lambda$  and  $\bar{\Lambda}$  are shown in Fig. 4. The  $\Lambda$  yield shows a behaviour which is almost independent of  $E_\nu$ ,  $W^2$  and  $Q^2$  after a sharp initial rise. It drops at large values of  $x_{Bj}$ . On the other hand, the yield of  $K_s^0$  rises steadily with  $E_\nu$  and  $W^2$ , reaches a plateau at large  $Q^2$  and falls with increasing  $x_{Bj}$ . Similar observations have been made by previous experiments, but with larger statistical uncertainties. The  $\bar{\Lambda}$  yields as a function of kinematic variables are measured for the first time in a neutrino experiment. In general

Table 7: Inclusive yields of neutral strange particles in  $\nu_\mu$  CC interactions measured in this analysis and in previous bubble chamber experiments.  $N_K$ ,  $N_\Lambda$  and  $N_{\bar{\Lambda}}$  are the observed numbers of  $K_s^0$ ,  $\Lambda$  and  $\bar{\Lambda}$ , respectively.  $K^0$  stands for  $K^0 + \bar{K}^0$ . See text for explanation of a star ( $\star$ ).

Reaction [Ref]	$\langle E_\nu \rangle$ (GeV)	$N_{K_s^0}$	$K^0$ rate (%)	$N_\Lambda$	$\Lambda$ rate (%)	$N_{\bar{\Lambda}}$	$\Lambda$ rate (%)
NOMAD	45	15075	$13.52 \pm 0.12$	8087	$5.04 \pm 0.06$	649	$0.37 \pm 0.02$
NOMAD $\star$			$18.22 \pm 0.16$		$6.66 \pm 0.08$		$0.45 \pm 0.02$
$\nu$ - Ne [19]	46	2279	$16.8 \pm 1.2$	1843	$6.5 \pm 0.5$	93	$0.46 \pm 0.08$
$\nu$ - p [24]	51	831	$19.0 \pm 0.9$	491	$5.2 \pm 0.3$	27	$0.34 \pm 0.07$
$\nu$ - Ne [25]	150	502	$40.8 \pm 4.8$	285	$12.7 \pm 1.4$	27	$1.5 \pm 0.5$
$\nu$ - p [11]	43	359	$17.5 \pm 0.9$	180	$4.5 \pm 0.4$	13	$0.3 \pm 0.1$
$\nu$ - Ne [12]	103	203	$23.0 \pm 1.7$	98	$5.7 \pm 0.7$		
$\nu$ - n [14]	62	234	$20.8 \pm 1.6$	157	$7.1 \pm 0.7$		
$\nu$ - p [14]	62	154	$17.7 \pm 1.6$	77	$4.3 \pm 0.6$		
$\nu$ - n [17]	62		$20.5 \pm 1.1$		$6.6 \pm 0.7$		
$\nu$ - p [17]	62		$17.4 \pm 1.2$		$4.4 \pm 0.5$		
$\nu$ - A [21]	$\sim 10$	82	$7.1 \pm 0.8$	76	$3.1 \pm 0.4$		
$\nu$ - p [10]	$\sim 45$	23	$15 \pm 4$				
$\nu$ - p [15]	$\sim 50$				$7.0 \pm 0.8$		
$\nu$ - n [15]	$\sim 50$				$7.0 \pm 1.2$		

they show a behaviour similar to that of the  $K_s^0$ . However, as expected, clear  $W^2$  and  $E_\nu$  thresholds are present in the  $\bar{\Lambda}$  production.

The ratios of yields for  $K_s^0/\Lambda$  and  $\bar{\Lambda}/\Lambda$  are presented in Fig. 5.

### 3.3 Comparison with LUND model predictions

The measured yields of  $K_s^0$ ,  $\Lambda$  and  $\bar{\Lambda}$  particles are compared in Figs. 6, 7, 8 to the predictions of the default NOMAD MC simulation (see section 2.1). A reasonable agreement in shapes is observed, while the discrepancy in the overall normalization is about a factor of 1.3 to 1.5.

The kinematic variables  $E_\nu$ ,  $W^2$ ,  $Q^2$  and  $x_{Bj}$  are not independent. So, for example, discrepancies between the data and MC at high  $W^2$  are reflected in discrepancies at low  $x_{Bj}$ .

## 4 PRODUCTION PROPERTIES

We have also performed a detailed analysis of kinematic quantities describing the behaviour of neutral strange particles ( $K_s^0$ ,  $\Lambda$  and  $\bar{\Lambda}$ ) inside the hadronic jet. This study allows an investigation of the dynamics of fragmentation. The differences in the production properties of  $K_s^0$ ,  $\Lambda$  and  $\bar{\Lambda}$  are seen most clearly here. The following distributions are of interest:  $x_F = 2p_L^*/W$  (Feynman- $x$  is the longitudinal momentum fraction in the hadronic center of mass system), the transverse momentum squared,  $p_T^2$ , of a particle with respect to the current (hadronic jet) direction and the fraction  $z = E_{lab}(V^0)/E_{lab}$  (all hadrons) of the total hadronic energy carried away by the neutral strange particle in the laboratory system.

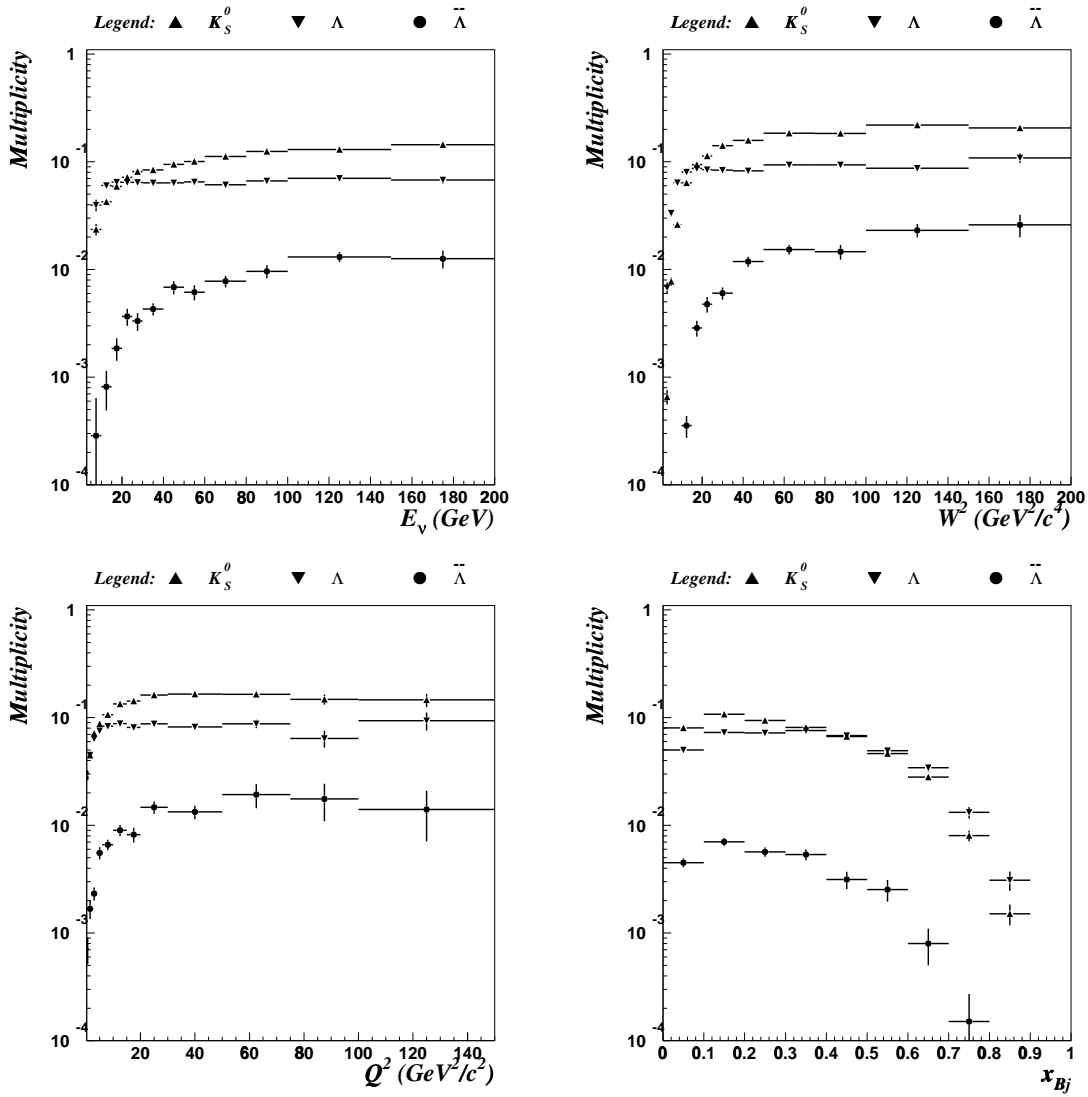


Figure 4: Measured yields of the  $K_s^0$ ,  $\Lambda$  and  $\bar{\Lambda}$  as a function of  $E_\nu$ ,  $W^2$ ,  $Q^2$  and  $x_{Bj}$ .

#### 4.1 $x_F$ distributions

The efficiency corrected  $x_F$  distributions observed in the data for neutral strange particles are shown in Figs. 9, 10, 11. These distributions indicate that  $\Lambda$  are produced mainly in the target fragmentation region ( $x_F < 0$ ), while  $K_s^0$  are peaked in the central region with an asymmetry in the forward direction.  $\bar{\Lambda}$  are produced in the central  $x_F$  region ( $|x_F| < 0.5$ ). One way to quantify differences in the  $x_F$  distributions is to define an asymmetry parameter  $A = (N_F - N_B)/(N_F + N_B)$ , where  $N_F$  and  $N_B$  are the numbers of particles produced forward and backward, respectively, in the hadronic centre of mass. The asymmetry parameters  $A$  and mean values of  $x_F$  in both data and MC are listed in Table 8. They are consistent with previous measurements [11, 12, 14, 19, 23, 24, 25]. The observed disagreement between data and MC is probably due to the fact that the MC simulation does not properly describe the relative contributions of different  $V^0$  production mechanisms.

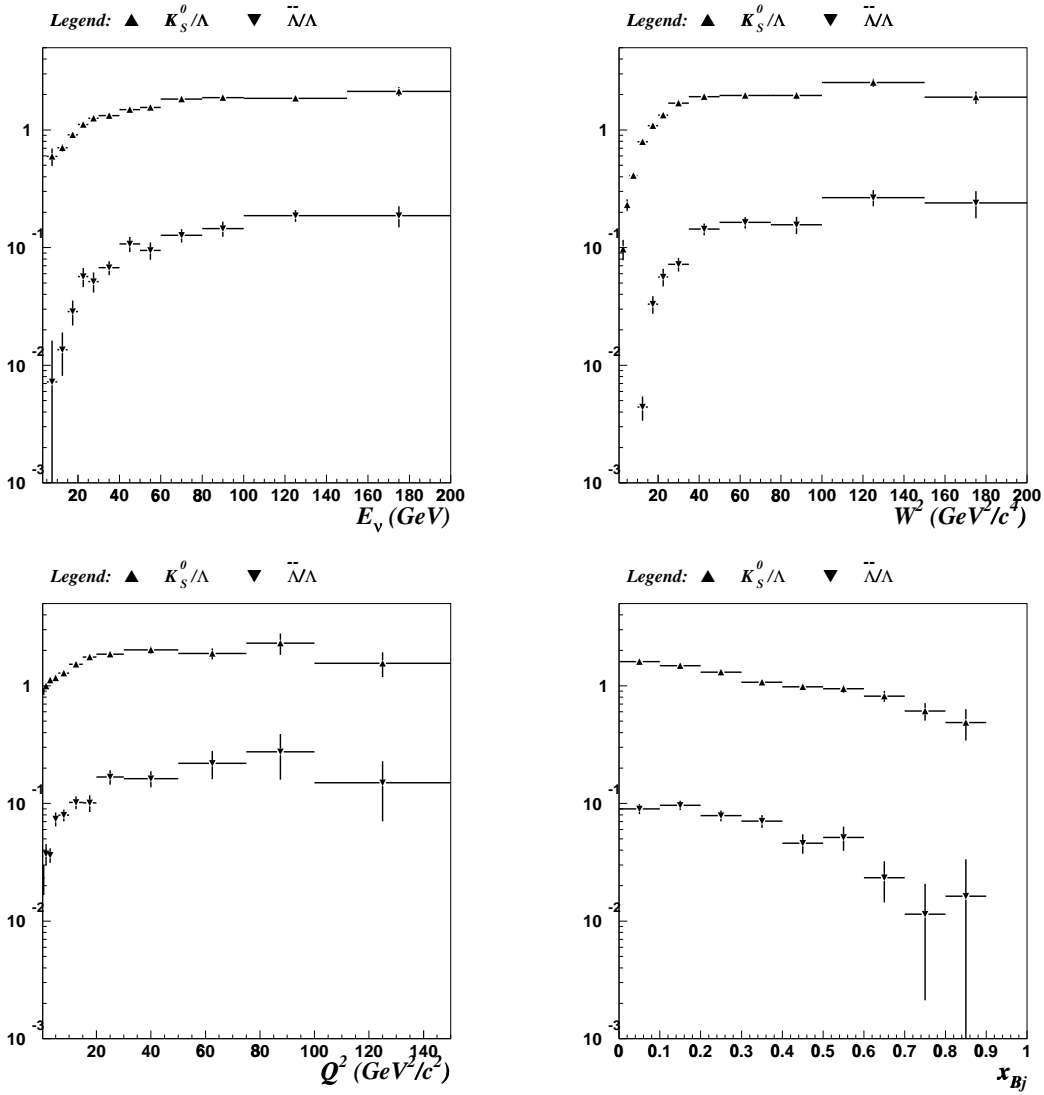


Figure 5: Ratios of measured yields for  $K_s^0/\Lambda$  and  $\bar{\Lambda}/\Lambda$  as a function of  $E_\nu$ ,  $W^2$ ,  $Q^2$  and  $x_{Bj}$ .

## 4.2 $z$ distributions

Efficiency corrected  $z$  distributions for  $K_s^0$ ,  $\Lambda$  and  $\bar{\Lambda}$  are shown in Figs. 12, 13, 14. A turn-over at small values of  $z$  can be seen for  $\bar{\Lambda}$  hyperons, but not for  $K_s^0$  and  $\Lambda$ . A turn-over at small values of  $z$  for  $K_s^0$  and  $\Lambda$  was observed in some of the previous neutrino experiments [8, 11, 14, 21] and was not observed in others [10, 12]. We note that uncorrected  $z$  distributions show such a turn-over for all  $V^0$  types in our experiment as well, due to a less efficient  $V^0$  reconstruction at low momenta.

Below we study separately  $z$  distributions of neutral strange particles produced at  $x_F < 0$  (see § 4.2.1) and at  $x_F > 0$  (see § 4.2.2). Detailed information on the mean values of  $z$  distributions for both data and MC is given in Table 9.

### 4.2.1 $z$ distributions in the target fragmentation region

The efficiency corrected  $z$  distributions of  $K_s^0$ ,  $\Lambda$  and  $\bar{\Lambda}$  measured in the target fragmentation region are shown in Fig. 15 (left). One can see that the  $z$  distribution of  $K_s^0$  mesons has a maximum at  $z \rightarrow 0$  and decreases faster at larger  $z$  (compared with Fig. 12)

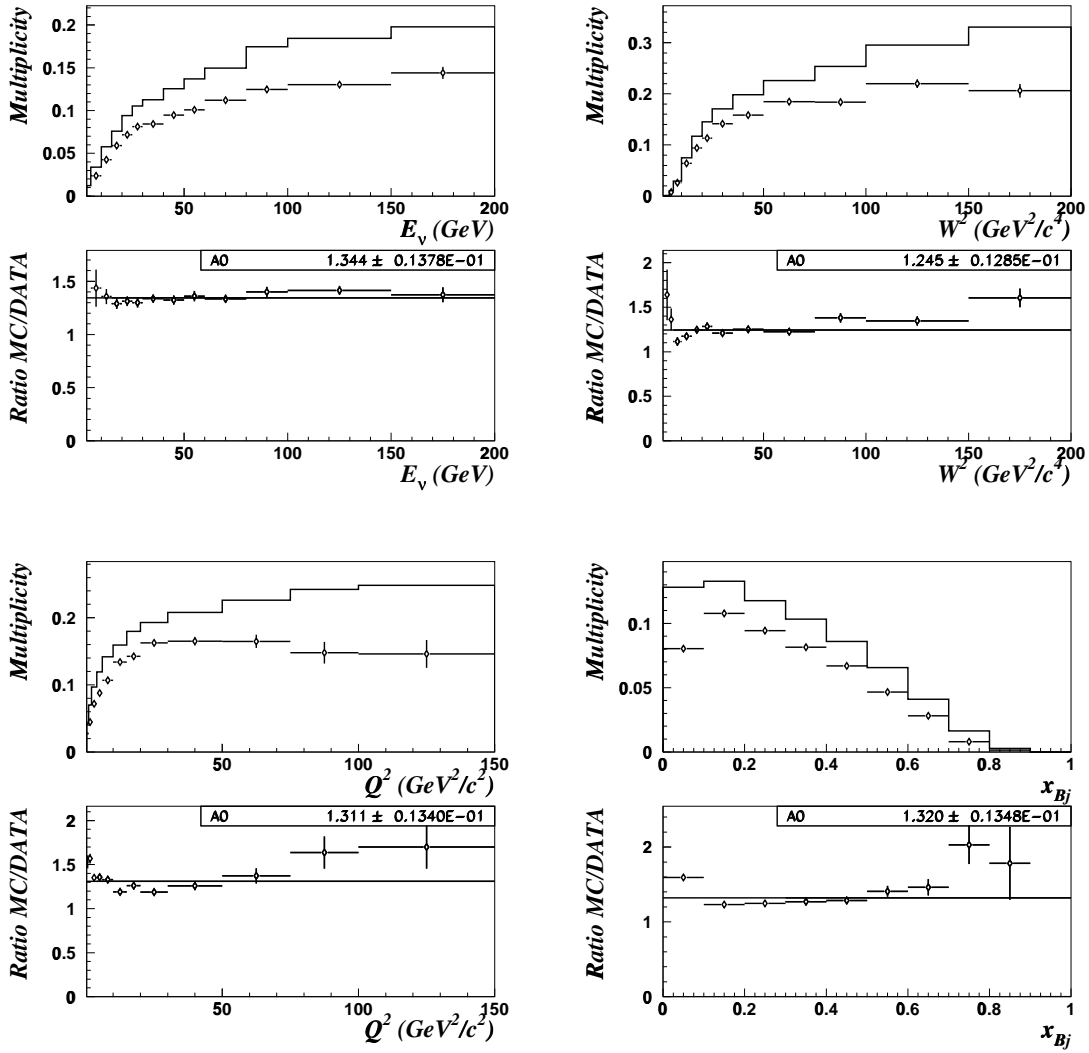


Figure 6: Yields in the default MC (histogram) and in the data (points with error bars) for  $K_s^0$  as a function of  $E_\nu$ ,  $W^2$ ,  $Q^2$  and  $x_{Bj}$ . The MC/Data ratios and their fit to a constant are also shown.

and that the  $K_s^0$  mesons produced in the target fragmentation region carry in general a small fraction of the hadronic jet energy.  $\Lambda$  hyperons are believed to be produced mostly from the remnant di-quark fragmentation and the shape of the  $z$  distribution is similar to that shown in Fig. 13. The turn-over in the  $z$  distribution is observed for  $\bar{\Lambda}$  hyperons produced in the target fragmentation region.

#### 4.2.2 $z$ distributions in the current fragmentation region

The efficiency corrected  $z$  distributions of  $K_s^0$ ,  $\Lambda$  and  $\bar{\Lambda}$  measured in the current fragmentation region are shown in Fig. 15 (right). This kinematical region is interesting because of the  $u$  or  $\bar{d}$  (anti)quark fragmentation into  $\Lambda$  or  $\bar{\Lambda}$  hyperons. All three  $z$  distributions show similar behaviour but with different mean values of  $z$ . The  $z$  distribution of  $\Lambda$  hyperons at  $x_F > 0$  is drastically different from that in the target fragmentation region. This is evidence for the fragmentation of the outgoing  $u$  quark into a  $\Lambda$  hyperon. In fact, the  $z$  distribution of  $\Lambda$  in the current fragmentation region is a measure of the

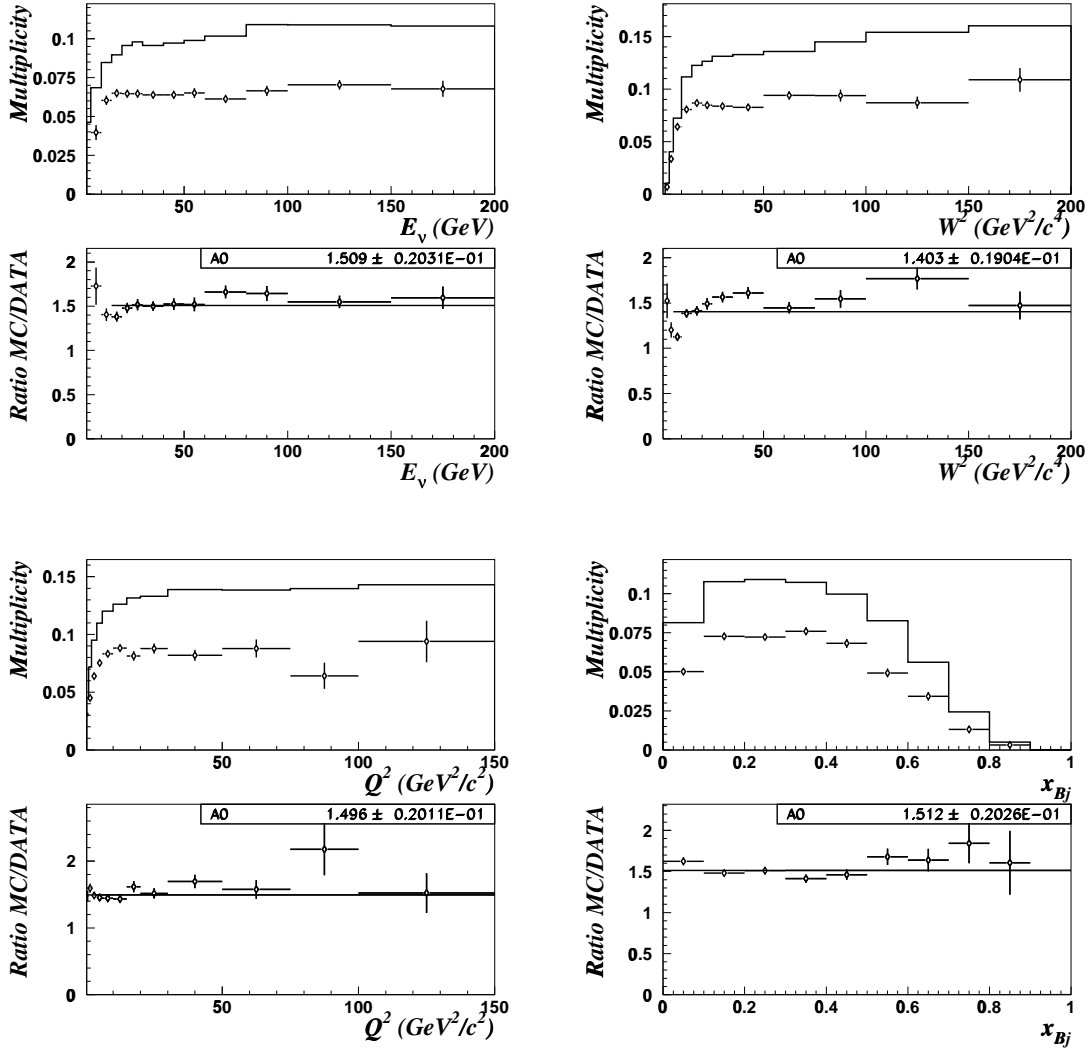


Figure 7: Yields in the default MC (histogram) and in the data (points with error bars) for  $\Lambda$  as a function of  $E_\nu$ ,  $W^2$ ,  $Q^2$  and  $x_{Bj}$ . The MC/Data ratios and their fit to a constant are also shown.

$D_u^\Lambda(z)$  fragmentation function (normalized to unity in Fig. 15). The  $z$  distribution of  $\bar{\Lambda}$  hyperons is sensitive to the  $D_d^{\bar{\Lambda}}(z)$  fragmentation function with a possible contribution from the  $D_u^{\bar{\Lambda}}(z)$  process. One can see that it is harder than the one measured in the target fragmentation region.

### 4.3 Discussion

There are different mechanisms responsible for  $K_s^0$ ,  $\Lambda$  and  $\bar{\Lambda}$  production in the neutrino CC DIS process which are expected to give different  $x_F$  and  $z$  distributions for these particles.

- The  $x_F$  distribution of  $K_s^0$  mesons produced promptly in the  $W^+d \rightarrow u$  process that requires at least two quark-antiquark pairs to be created ( $d\bar{d}$  and  $s\bar{s}$ ) is expected to be central. A contribution from heavier strange particle decays (mainly from  $K^{*+}$ ) produced from the fragmentation of the outgoing  $u$  quark can result in a forward  $x_F$  distribution for  $K_s^0$  mesons. Also  $K_s^0$  mesons from a fragmentation of the outgoing

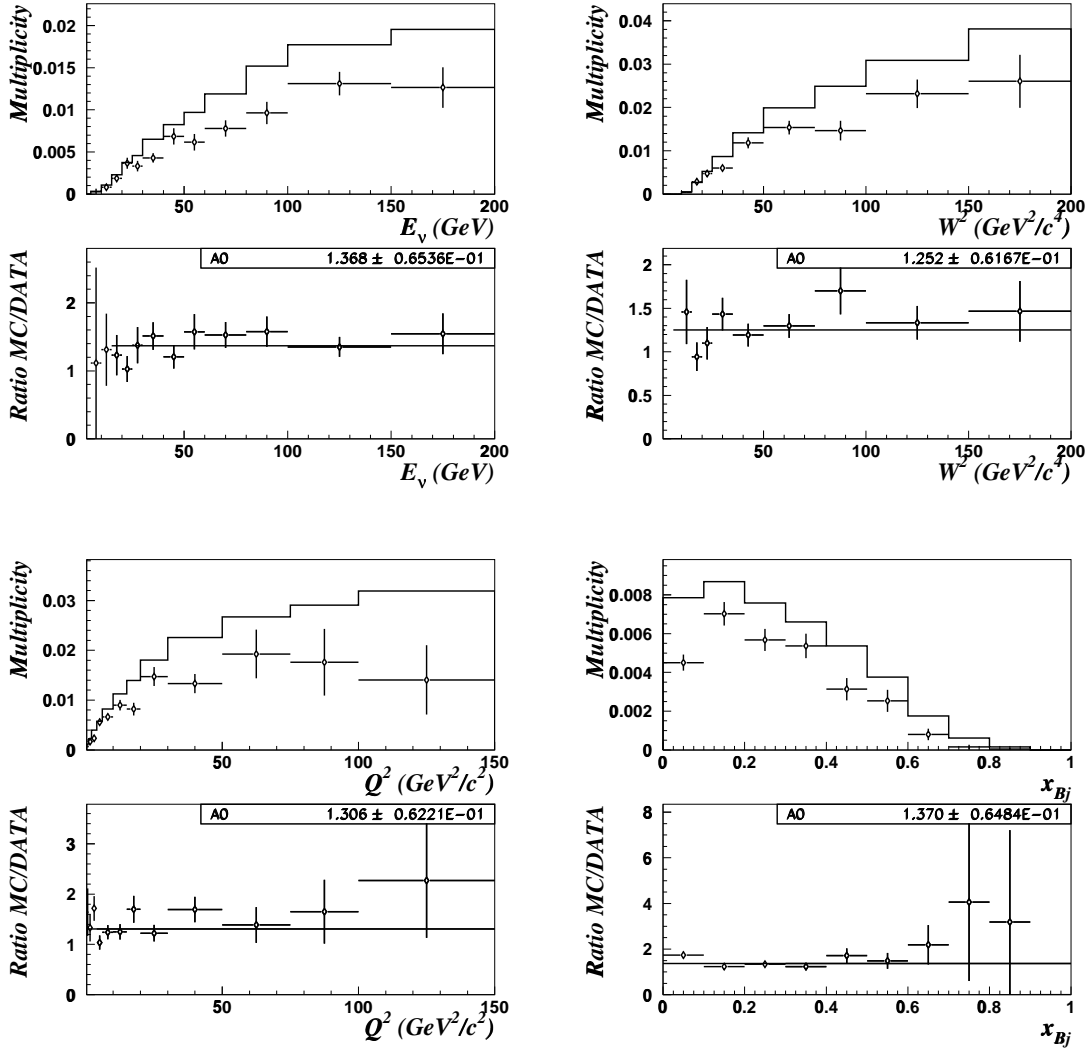


Figure 8: Yields in the default MC (histogram) and in the data (points with error bars) for  $\bar{\Lambda}$  as a function of  $E_\nu$ ,  $W^2$ ,  $Q^2$  and  $x_{Bj}$ . The MC/Data ratios and their fit to a constant are also shown.

(anti)quark in  $W^+d \rightarrow c \rightarrow s$  and  $W^+\bar{u} \rightarrow \bar{d}$  processes are expected to be produced in the forward  $x_F$  region and to carry a larger fraction of the jet energy.

- $\Lambda$  hyperons can be produced from the fragmentation of the nucleon di-quark remnant promptly and via the decay of heavier strange baryons at  $x_F < 0$ .  $\Lambda$  hyperons can be produced also at  $x_F > 0$  from the outgoing  $u$  quark fragmentation.
- The production of  $\bar{\Lambda}$  hyperons in neutrino scattering from a valence quark requires three quark-antiquark pairs to be created ( $u\bar{u}$ ,  $d\bar{d}$  and  $s\bar{s}$ ) and is expected to populate the central region of the  $x_F$  distribution. There could also be a contribution from the outgoing antiquark fragmentation into a  $\bar{\Lambda}$  hyperon (in the  $W^+\bar{u} \rightarrow \bar{d} \rightarrow \bar{\Lambda}$  process) which can produce these baryons in the forward  $x_F$  region.

#### 4.4 $p_T^2$ distributions

The efficiency corrected  $p_T^2$  distributions of  $K_s^0$ ,  $\Lambda$  and  $\bar{\Lambda}$  in the data are presented in Figs. 16, 17, 18. They show an exponential behaviour of the form  $C \exp(-B \cdot p_T^2)$  in



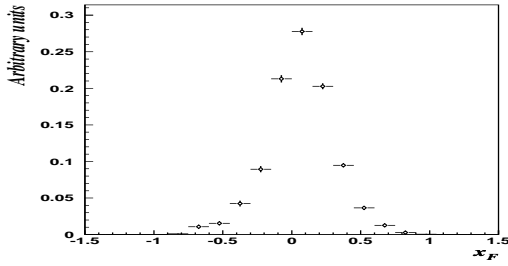


Figure 9: *Efficiency corrected  $x_F$  distribution for  $K_s^0$  mesons.*

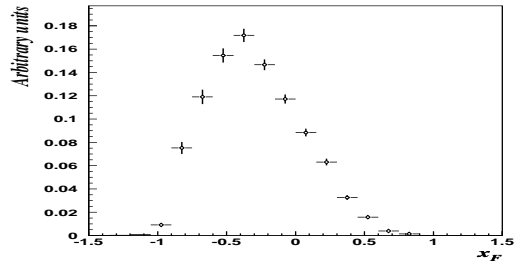


Figure 10: *Efficiency corrected  $x_F$  distribution for  $\Lambda$  hyperons.*

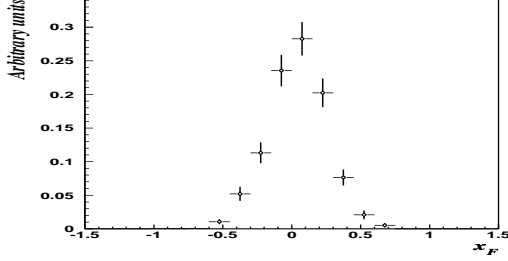


Figure 11: *Efficiency corrected  $x_F$  distribution for  $\bar{\Lambda}$  hyperons.*

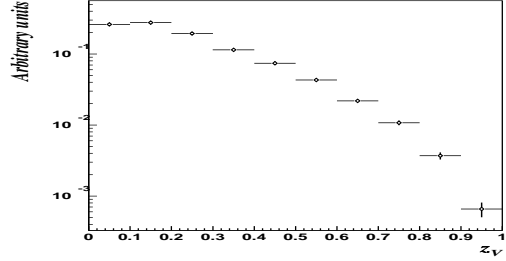


Figure 12: *Efficiency corrected  $z$  distribution for  $K_s^0$ .*

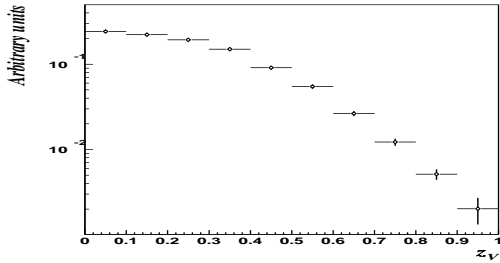


Figure 13: *Efficiency corrected  $z$  distributions for  $\Lambda$ .*

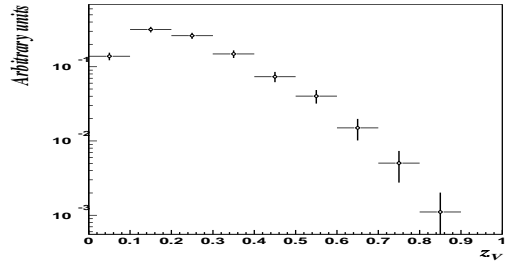


Figure 14: *Efficiency corrected  $z$  distributions for  $\bar{\Lambda}$ .*

the region  $p_T^2 \lesssim 0.5$  ( $\text{GeV}^2/c^2$ ) and a deviation from this dependence at higher  $p_T^2$ . We measured the slope parameter  $B$  in the region  $0 < p_T^2 < 0.5$   $\text{GeV}^2/c^2$  for each  $V^0$  category in three kinematic regions: all  $x_F$ ,  $x_F < 0$  and  $x_F > 0$ . The results are listed in Table 10. The values of the slope parameter found in different  $x_F$  regions are similar, except for  $\bar{\Lambda}$  hyperons.

#### 4.5 $\langle p_T^2 \rangle$ versus $x_F$ distributions

We have also studied the dependence of the average  $\langle p_T^2 \rangle$  on  $x_F$  for  $K_s^0$ ,  $\Lambda$  and  $\bar{\Lambda}$  (see Figs. 19, 20, 21). For the first time in a neutrino experiment the good quality of event reconstruction combined with the large statistics of the data collected allows the study of these distributions for neutral strange particles<sup>2)</sup>. The observed discrepancy

<sup>2)</sup> Similar distributions obtained for charged particles in bubble chamber neutrino experiments [47] have been used to tune Monte Carlo simulation programs.

Table 8: Mean values  $\langle x_F \rangle$  and asymmetry parameters  $A$  of the  $x_F$  distributions for  $K_s^0$ ,  $\Lambda$ ,  $\bar{\Lambda}$  in both MC and data.

$V^0$	MC		DATA	
	$\langle x_F \rangle$	A	$\langle x_F \rangle$	A
$K_s^0$	$0.055 \pm 0.001$	$0.152 \pm 0.002$	$0.064 \pm 0.001$	$0.256 \pm 0.004$
$\Lambda$	$-0.296 \pm 0.001$	$-0.649 \pm 0.002$	$-0.295 \pm 0.002$	$-0.589 \pm 0.004$
$\bar{\Lambda}$	$0.006 \pm 0.002$	$-0.03 \pm 0.01$	$0.04 \pm 0.004$	$0.18 \pm 0.02$

Table 9: Mean values of  $z$  distributions for  $K_s^0$ ,  $\Lambda$ ,  $\bar{\Lambda}$  measured for the full sample and for  $x_F < 0$  and  $x_F > 0$  regions in both MC and data.

$V^0$		full sample	$x_F < 0$	$x_F > 0$
$K_s^0$	MC	$0.218 \pm 0.001$	$0.092 \pm 0.001$	$0.312 \pm 0.001$
	DATA	$0.226 \pm 0.001$	$0.105 \pm 0.001$	$0.299 \pm 0.001$
$\Lambda$	MC	$0.227 \pm 0.001$	$0.179 \pm 0.001$	$0.462 \pm 0.003$
	DATA	$0.250 \pm 0.002$	$0.206 \pm 0.001$	$0.434 \pm 0.005$
$\bar{\Lambda}$	MC	$0.215 \pm 0.003$	$0.139 \pm 0.002$	$0.296 \pm 0.004$
	DATA	$0.242 \pm 0.005$	$0.147 \pm 0.005$	$0.308 \pm 0.008$

between the data and simulated events in the region  $x_F \gtrsim 0.3$  could be attributed to the absence of QCD effects in our Monte Carlo simulation program: the so-called soft-gluon effect could change the leading particle ( $x_F \rightarrow 1$ ) behaviour inside the hadronic jet since the forward scattered quark is strongly accelerated and is therefore expected to radiate gluons, thus broadening the forward  $p_T^2$  distribution. It has also been verified that there is no accumulation of misidentified  $V^0$  in the region where the disagreement between the MC simulation and the data is observed.

## 5 STRANGE RESONANCES AND HEAVIER HYPERONS

Apart from many good physics reasons a study of the production of resonances and heavy hyperons is also of great importance for tuning the LUND model parameters and for the theoretical interpretation of the  $\Lambda$  and  $\bar{\Lambda}$  polarization measurements reported in our previous articles [27, 28]. This is essential because  $\Lambda$  hyperons originating from the

Table 10: The slope parameter  $B(\text{GeV}/c)^{-2}$  of the  $p_T^2$  distribution for  $K_s^0$ ,  $\Lambda$ ,  $\bar{\Lambda}$  measured separately for the full sample and for  $x_F < 0$  and  $x_F > 0$  regions in both MC and in data.

$V^0$	MC			DATA		
	full sample	$x_F < 0$	$x_F > 0$	full sample	$x_F < 0$	$x_F > 0$
$K_s^0$	$5.72 \pm 0.03$	$5.61 \pm 0.04$	$5.79 \pm 0.03$	$5.21 \pm 0.10$	$5.40 \pm 0.21$	$5.15 \pm 0.11$
$\Lambda$	$4.35 \pm 0.03$	$4.30 \pm 0.03$	$4.58 \pm 0.06$	$4.12 \pm 0.13$	$4.18 \pm 0.15$	$4.07 \pm 0.27$
$\bar{\Lambda}$	$3.89 \pm 0.10$	$4.10 \pm 0.13$	$3.70 \pm 0.14$	$4.42 \pm 0.47$	$6.59 \pm 0.74$	$3.30 \pm 0.64$

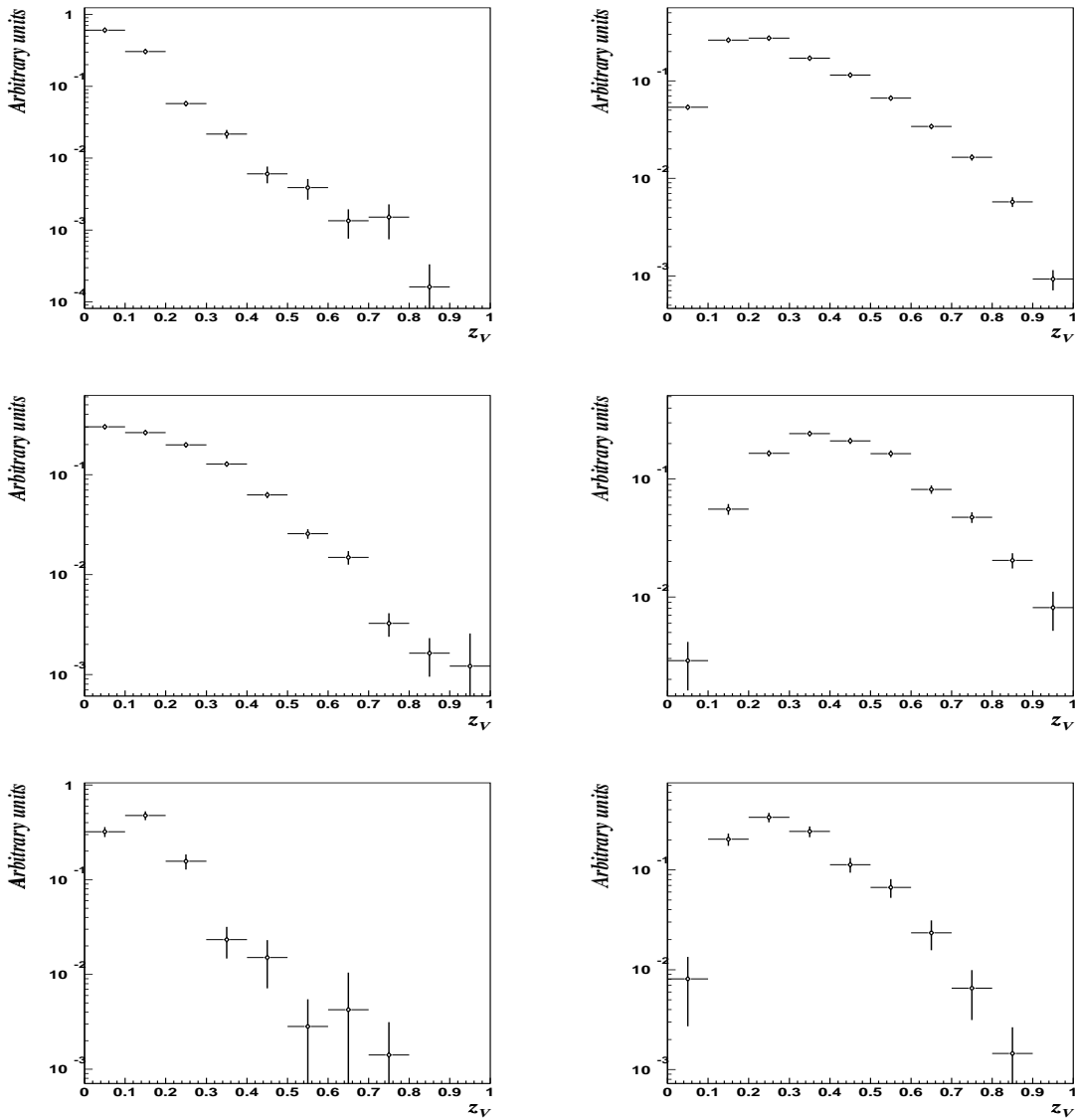


Figure 15: *Efficiency corrected  $z$  distributions for  $x_F < 0$  (left) and for  $x_F > 0$  (right) for  $K_s^0$  (top),  $\Lambda$  (centre) and  $\bar{\Lambda}$  (bottom).*

decays  $\Sigma^* \rightarrow \Lambda\pi$ ,  $\Sigma^0 \rightarrow \Lambda\gamma$  and  $\Xi \rightarrow \Lambda\pi$  inherit a polarization from the parent particles and this polarization is different from that of a directly produced  $\Lambda$ . Information about  $\Sigma^0$ ,  $\Xi$ ,  $\Sigma^*$ ,  $\Xi^*$  and  $K^*$  yields can be obtained from an analysis of their decays into channels containing identified neutral strange particles [39, 48].

Previous bubble chamber experiments with (anti)neutrino beams suffered from a lack of statistics. For example, the BEBC WA21 Collaboration [24] reported the observation of  $149 \pm 29 K^{*+}$ ,  $42 \pm 19 K^{*-}$ ,  $134 \pm 19 \Sigma^{*+}$  and less than 10  $\Sigma^{*-}$  in  $\nu_\mu p$  CC interactions, while the Fermilab 15-ft bubble chamber E380 Collaboration [19] found  $94 \pm 25 \Sigma^0$  and 4  $\Xi^-$  in  $\nu_\mu \text{Ne}$  CC events.

### 5.1 A procedure for signal extraction

Our aim was to extract the fraction of neutral strange particles which are decay products of resonances and heavier hyperons from the corresponding invariant mass dis-

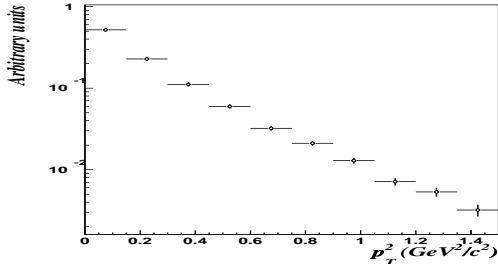


Figure 16: Efficiency corrected  $p_T^2$  distribution for  $K_s^0$ .

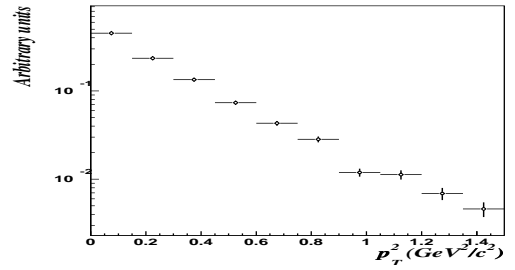


Figure 17: Efficiency corrected  $p_T^2$  distribution for  $\Lambda$ .

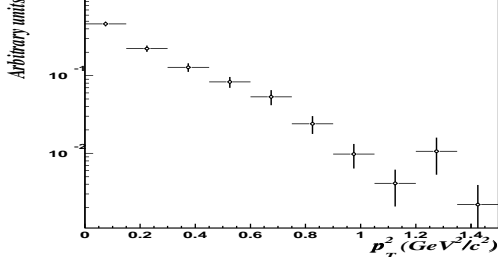


Figure 18: Efficiency corrected  $p_T^2$  distribution for  $\bar{\Lambda}$ .

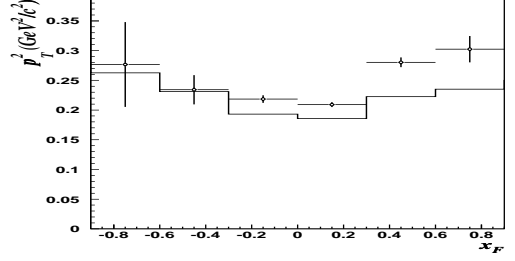


Figure 19: Efficiency corrected  $\langle p_T^2 \rangle$  versus  $x_F$  distribution for  $K_s^0$  in data (points with error bars) and MC (histogram).

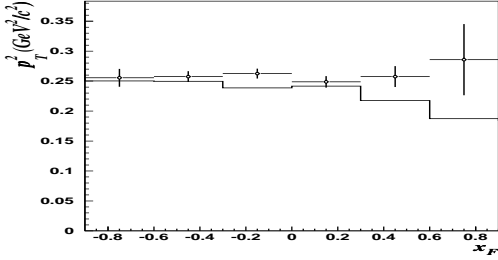


Figure 20: Efficiency corrected  $\langle p_T^2 \rangle$  versus  $x_F$  distribution for  $\Lambda$  in data (points with error bars) and MC (histogram).

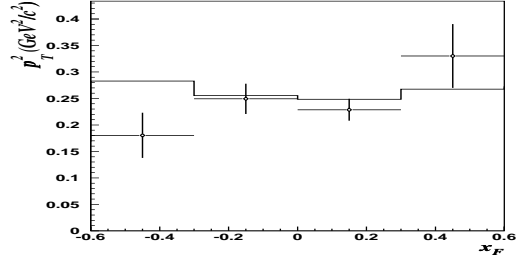


Figure 21: Efficiency corrected  $\langle p_T^2 \rangle$  versus  $x_F$  distribution for  $\bar{\Lambda}$  in data (points with error bars) and MC (histogram).

tributions. To construct such distributions we combine the neutral strange particle with all possible charged tracks (of appropriate sign) emerging from the primary vertex except those identified as muons or electrons. We have also studied the  $(\Lambda \gamma)$  combinations, where photons are identified as conversions in the detector fiducial volume via our  $V^0$  identification procedure. The resulting distributions are fitted by a function describing both the combinatorial background and the resonance signal.

The combinatorial background (BG) can be approximated by any function of the form:

$$BG = P_n(m - M_{th}) \cdot Tail(m), \quad (2)$$

where  $P_n(m - M_{th})$  is a polynomial of order  $n$  vanishing at  $m = M_{th}$ ,  $M_{th} = M_{V^0} + m_\pi$ , and  $Tail(m)$  is any function vanishing at  $m \rightarrow \infty$  faster than  $P_n$  increases.

We have chosen the following BG parametrization:

$$BG = a_1 \Delta^{a_2} e^{-(a_3 \Delta + a_4 \Delta^2)}, \quad (3)$$

where  $\Delta = m - M_{th}$ .

For a resonance signal the standard relativistic Breit-Wigner (BW) function [49] is used:

$$BW(m) = \frac{\Gamma}{(m^2 - M_0^2)^2 + M_0^2 \Gamma^2} \left( \frac{m}{q} \right), \quad \text{with} \quad \Gamma = \Gamma_0 \left( \frac{q}{q_0} \right) \frac{M_0}{m} \quad (4)$$

where  $M_0, \Gamma_0$  are the resonance mass and width, respectively, and  $q$  is the momentum of the decay product in the resonance rest frame ( $q_0$  corresponds to  $M_0$ ).

Finally, we have fitted the invariant mass distributions by:

$$\frac{dN}{dm} = BG(\Delta) + a_5 BW'(m), \quad (5)$$

for all combinations except  $(\Lambda \pi^-)$ , where two peaks due to  $\Sigma^{*-} \rightarrow \Lambda \pi^-$  and  $\Xi^- \rightarrow \Lambda \pi^-$  decays are expected. Here  $BW'(m)$  is the Breit-Wigner function of equation (4) normalized to unity. Such a fit is valid in all cases when the experimental mass resolution is small compared with the natural width of the resonance.

Similarly, for the  $(\Lambda \pi^-)$  case we have used

$$\frac{dN}{dm} = BG(\Delta) + a_5 BW'_{\Sigma^{*-}}(m) + a_6 BW'_{\Xi^-}(m) \quad (6)$$

where the invariant mass resolution is used for the width  $\Gamma_0$  in the Breit-Wigner function corresponding to the  $\Xi^-$  decay. In the above formulae  $a_1$  to  $a_6$  are parameters of the fit.

In such an approach using the HESSE and MINOS procedures of MINUIT [50], the parameter  $a_5(a_6)$  gives the number of signal events with the corresponding error which takes into account possible correlations between different parameters.

As a consistency check we have also tried an alternative approach which was to fit the invariant mass distributions with:

$$\frac{dN}{dm} = (1 + a_5 BW(m)) BG(\Delta), \quad (7)$$

and, similarly, with

$$\frac{dN}{dm} = (1 + a_5 BW_{\Sigma^{*-}}(m) + a_6 BW_{\Xi^-}(m)) BG(\Delta), \quad (8)$$

and extracted the corresponding number of signal events.

The results obtained using these two approaches were found to be similar. In what follows we present our results using the first method.

## 5.2 Results

The yields of resonances and heavy hyperons have been studied in different kinematic regions and for neutrino interactions on different target nucleons.

In NOMAD it is to some extent possible to separate neutrino interactions on the neutrons and protons by imposing a cut on the sum of charges ( $Q_{tot}$ ) of all the outgoing tracks at the primary neutrino interaction vertex.

We select  $\nu p$  events requiring  $Q_{tot} \geq 1$ . According to the MC simulation, in this proton-like sample 76% of the events are true  $\nu p$  interactions. The  $\nu n$  events are selected by the requirement  $Q_{tot} \leq 0$ . The purity of the corresponding neutron-like sample is about 85%.

Since the hadron production mechanisms in the target and in the current fragmentation regions are expected to be different, it is important to study separately the yields of resonances and heavy hyperons at  $x_F < 0$  and  $x_F > 0$ . Such a study is also necessary for a correct theoretical interpretation of the  $\Lambda$  ( $\bar{\Lambda}$ ) polarization measurements reported in our previous papers [27, 28].

In the following we denote as MC(pred.) the true number of heavy strange particles reconstructed in the MC, and MC(meas.) the number of heavy strange particles extracted from the MC sample using our fitting procedure. Both quantities are normalized to the number of  $\nu_\mu$  CC events in the data.

Note that MC(pred.) and MC(meas.) can be slightly different due to limitations of the signal extraction procedure described in section 5.1. The threshold and smearing effects in the invariant mass distributions are at the origin of this discrepancy. The ratio MC(pred.)/MC(meas.) will therefore be used to correct the yields of heavy strange particles extracted from the data (see section 5.3).

The following resonances and heavier hyperons have been studied in the present analysis.

### 5.2.1 $K^{*\pm}$

The fitted ( $K_s^0 \pi^\pm$ ) invariant mass distributions are shown in Fig. 22 for both MC and data samples. Detailed information on the number of extracted  $K^{*\pm}$  events and the  $K^{*\pm}/K_s^0$  ratio is given in Tables 11 and 12. For the  $K^{*\pm}$  mass and width we have used 891.66 MeV and 50.8 MeV respectively. The  $q_0$  value is 291 MeV/c [40].

Table 11:  $K^{*+} \rightarrow K_s^0 \pi^+$  *summary*

N( $K^{*+}$ )	full sample	$K_s^0$ fragmentation region		type of target nucleon	
		$x_F < 0$	$x_F > 0$	$\nu p$	$\nu n$
DATA	$2036 \pm 121$	$315 \pm 56$	$1731 \pm 108$	$1006 \pm 87$	$1032 \pm 84$
MC(meas.)	$5373 \pm 104$	$726 \pm 47$	$4744 \pm 93$	$1963 \pm 67$	$3516 \pm 80$
MC(pred.)	5953	886	5067	2206	3748
N( $K^{*+}$ )/N( $K_s^0$ )	uncorrected				
DATA (%)	$13.5 \pm 0.8$	$9.7 \pm 1.7$	$14.6 \pm 0.9$	$15.7 \pm 1.4$	$11.9 \pm 1.0$
MC (%)	$27.3 \pm 0.5$	$14.5 \pm 0.9$	$31.6 \pm 0.6$	$29.0 \pm 1.0$	$26.5 \pm 0.6$

It is interesting to note a more abundant  $K^{*+}$  than  $K^{*-}$  production in  $\nu_\mu$  CC DIS. This can be explained by the fact that the outgoing  $u$  quark can fragment directly into a  $K^{*+}$ , while both  $\bar{u}$  and  $s$  quarks needed to produce a  $K^{*-}$  meson have to be created in the fragmentation process.

One can see that there is a significant difference between  $K^{*\pm}$  yields in the default MC simulation and the NOMAD data (about a factor of 2).

### 5.2.2 $\Sigma^{*\pm}$

For the  $\Sigma^{*\pm}$  mass and width we have taken the values from [40]:  $m(\Sigma^{*+})=1382.8$  MeV,  $\Gamma(\Sigma^{*+})=35.8$  MeV,  $m(\Sigma^{*-})=1387.2$  MeV,  $\Gamma(\Sigma^{*-})=39.4$  MeV. The  $q_0$  value is 208

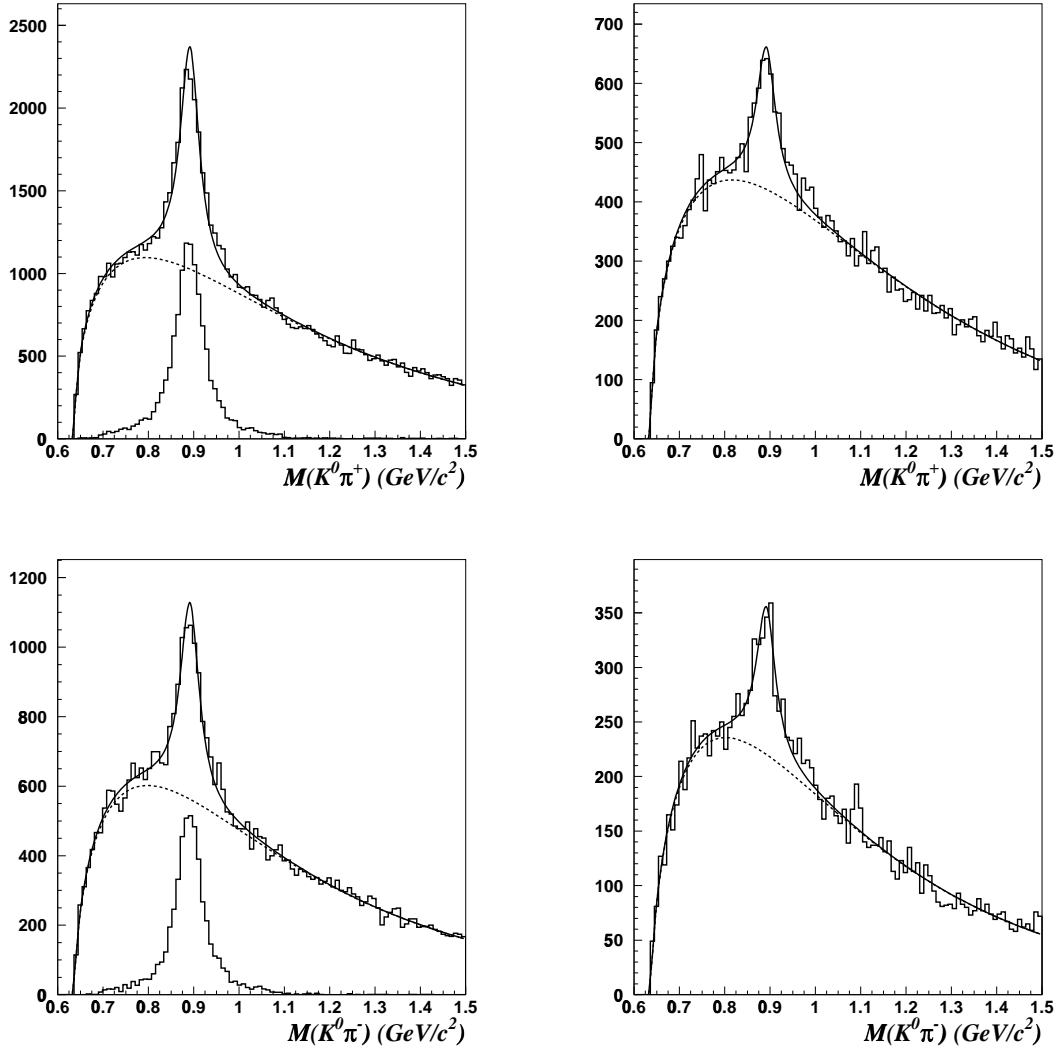


Figure 22:  $K_s^0\pi^+$  (top) and  $K_s^0\pi^-$  (bottom) invariant mass distributions for both MC (left) and data (right). The solid lines are the results of the fit, while the dotted lines describe the background term. In the MC plots the additional histograms refer to the reconstructed true heavy strange particles.

MeV/c.

The fitted invariant mass distributions for  $(\Lambda \pi^\pm)$  combinations in both MC and data samples are shown in Fig. 23. Detailed information on the number of extracted  $\Sigma^{*\pm}$  events and the  $\Sigma^{*\pm}/\Lambda$  ratio is given in Tables 13 and 14.

A striking difference between the  $\Sigma^{*\pm}$  yields in the default MC simulation and in the NOMAD data (a factor of about 3 or even larger) is observed.

### 5.2.3 $\Xi^-$

For the  $\Xi^-$  mass we have used 1321.32 MeV [40], for the width the experimental resolution of 10 MeV has been taken. The  $q_0$  value is 139 MeV/c.

The bottom plots in Fig. 23 show evidence for  $\Xi^- \rightarrow \Lambda\pi^-$  decays. Detailed information on the number of extracted  $\Xi^-$  events and the  $\Xi^-/\Lambda$  ratio is given in Table 15.

Table 12:  $K^{*-} \rightarrow K_s^0 \pi^-$  summary

N( $K^{*-}$ )	full sample	$K_s^0$ fragmentation region		type of target nucleon	
		$x_F < 0$	$x_F > 0$	$\nu p$	$\nu n$
DATA	$1146 \pm 89$	$288 \pm 44$	$865 \pm 78$	$377 \pm 52$	$775 \pm 73$
MC(meas.)	$2304 \pm 74$	$639 \pm 38$	$1664 \pm 63$	$729 \pm 39$	$1576 \pm 63$
MC(pred.)	2467	723	1743	734	1733
N( $K^{*-}$ )/N( $K_s^0$ )	uncorrected				
DATA (%)	$7.6 \pm 0.6$	$8.9 \pm 1.3$	$7.3 \pm 0.7$	$5.9 \pm 0.8$	$8.9 \pm 0.8$
MC (%)	$11.5 \pm 0.4$	$12.7 \pm 0.8$	$11.1 \pm 0.4$	$10.8 \pm 0.6$	$11.9 \pm 0.5$

Table 13:  $\Sigma^{*+} \rightarrow \Lambda \pi^+$  summary

N( $\Sigma^{*+}$ )	full sample	$\Lambda$ fragmentation region		type of target nucleon	
		$x_F < 0$	$x_F > 0$	$\nu p$	$\nu n$
DATA	$416 \pm 80$	$358 \pm 65$	$63 \pm 47$	$297 \pm 61$	$120 \pm 51$
MC(meas.)	$2070 \pm 68$	$1427 \pm 57$	$649 \pm 37$	$1321 \pm 49$	$754 \pm 46$
MC(pred.)	1783	1254	529	1150	634
N( $\Sigma^{*+}$ )/N( $\Lambda$ )	uncorrected				
DATA (%)	$5.2 \pm 1.0$	$6.4 \pm 1.2$	$2.5 \pm 1.9$	$8.6 \pm 1.8$	$2.6 \pm 1.1$
MC (%)	$17.0 \pm 0.6$	$15.9 \pm 0.6$	$20.6 \pm 1.2$	$32.6 \pm 1.2$	$9.3 \pm 0.6$

#### 5.2.4 $\Sigma^0$

For the  $\Sigma^0$  mass we have taken the value from [40]:  $m(\Sigma^0)=1192.6$  MeV, while for the width the experimental resolution of 9 MeV has been used. The  $q_0$  value is 74 MeV/c. The  $\Sigma^0$  peak has been fitted by a Gaussian function.

Fig. 24 shows the fitted invariant mass distributions for ( $\Lambda \gamma$ ) combinations in both Monte Carlo and data samples. The corresponding photons have been reconstructed as conversions in the DC fiducial volume and identified by our  $V^0$  identification procedure. The quality of the photon reconstruction is illustrated by the ( $\gamma\gamma$ ) invariant mass distributions shown in Fig. 25 for both MC and data: a peak corresponding to the  $\pi^0$  signal is evident.

A summary of the number of extracted  $\Sigma^0$  events and the  $\Sigma^0/\Lambda$  ratio is given in Table 16.

Table 14:  $\Sigma^{*-} \rightarrow \Lambda \pi^-$  summary

N( $\Sigma^{*-}$ )	full sample	$\Lambda$ fragmentation region		type of target nucleon	
		$x_F < 0$	$x_F > 0$	$\nu p$	$\nu n$
DATA	$206 \pm 63$	$121 \pm 51$	$93 \pm 37$	$100 \pm 35$	$111 \pm 52$
MC(meas.)	$551 \pm 48$	$410 \pm 42$	$145 \pm 25$	$18 \pm 22$	$528 \pm 43$
MC(pred.)	489	362	126	33	456
N( $\Sigma^{*-}$ )/N( $\Lambda$ )	uncorrected				
DATA (%)	$2.6 \pm 0.8$	$2.2 \pm 0.9$	$3.7 \pm 1.5$	$2.9 \pm 1.0$	$2.4 \pm 1.1$
MC (%)	$4.5 \pm 0.4$	$4.6 \pm 0.5$	$4.6 \pm 0.8$	$0.4 \pm 0.5$	$6.5 \pm 0.5$



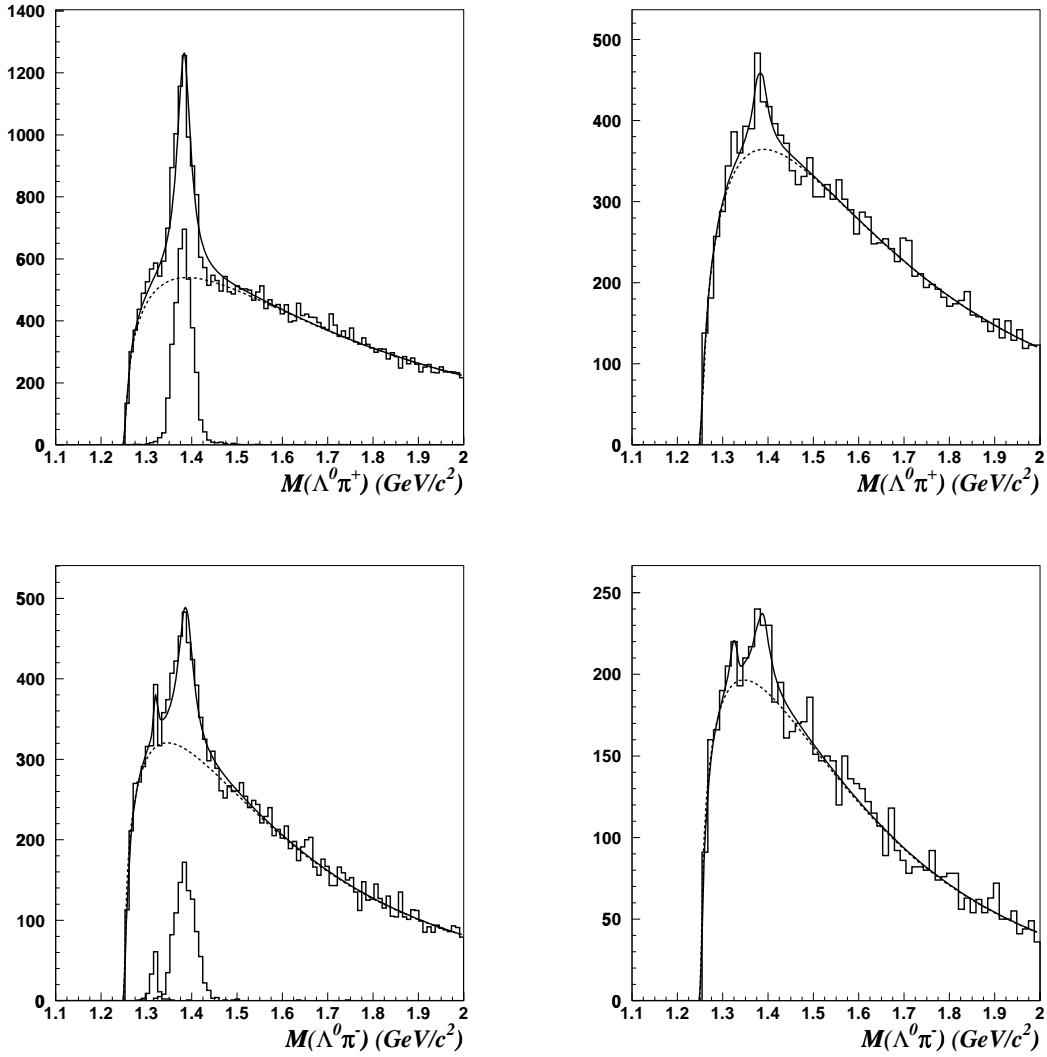


Figure 23:  $\Lambda\pi^+$  (top) and  $\Lambda\pi^-$  (bottom) invariant mass distributions for both MC (left) and data (right). The solid lines are the results of the fit, while the dotted lines describe the background term. In the MC plots the additional histograms refer to the reconstructed true heavy strange particles.

### 5.3 Yields of strange resonances and heavy hyperons

The integral yields of strange resonances and heavy hyperons produced in  $\nu_\mu$  CC are computed multiplying the results of the fits by the ratio  $\text{MC}(\text{pred.})/\text{MC}(\text{meas.})$ .

The results are presented in Table 17 as fractions of  $V^0$  produced by heavy strange particles and resonances.

### 5.4 Discussion

The results of our study confirm discrepancies reported earlier [14] in the description of the strange resonances and heavy hyperon production in neutrino interactions by the LUND model with default parameters [30, 31]. These results could be potentially used to tune the MC parameters responsible for the fragmentation into strange particles. Moreover, an additional analysis of events with multiple production of neutral strange particles could be very useful in this respect. Such an analysis is currently in progress.

Table 15:  $\Xi^- \rightarrow \Lambda\pi^-$  summary

N( $\Xi^-$ )	full sample	$\Lambda$ fragmentation region		type of target nucleon	
		$x_F < 0$	$x_F > 0$	$\nu p$	$\nu n$
DATA	$42 \pm 30$	$21 \pm 24$	$18 \pm 17$	$54 \pm 18$	$-11 \pm 24$
MC(meas.)	$43 \pm 18$	$33 \pm 15$	$13 \pm 9$	$9 \pm 8$	$36 \pm 16$
MC(pred.)	60	47	15	14	47
N( $\Xi^-$ )/N( $\Lambda$ )	uncorrected				
DATA (%)	$0.5 \pm 0.4$	$0.4 \pm 0.4$	$0.7 \pm 0.7$	$1.6 \pm 0.5$	$-0.2 \pm 0.5$
MC (%)	$0.4 \pm 0.2$	$0.4 \pm 0.2$	$0.4 \pm 0.3$	$0.2 \pm 0.2$	$0.4 \pm 0.2$

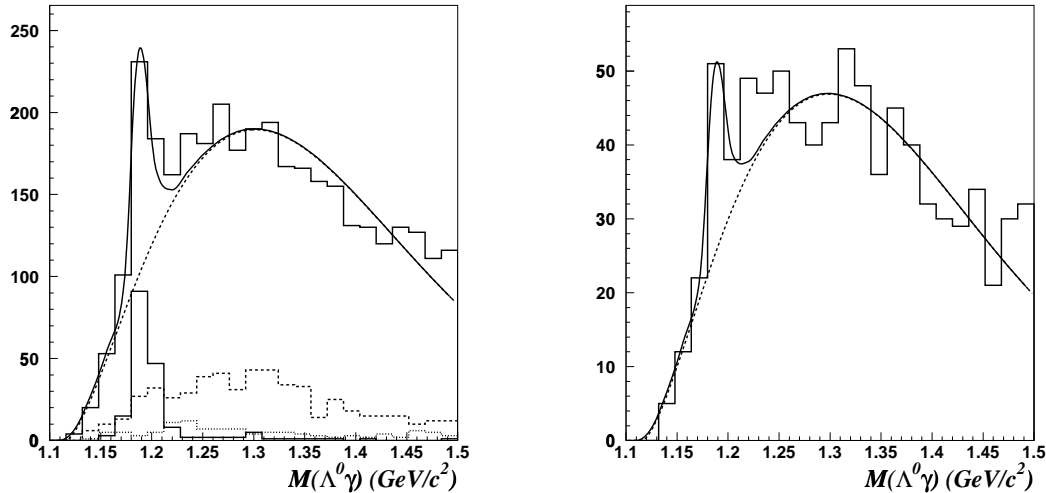


Figure 24:  $\Lambda\gamma$  invariant mass distributions for both MC (left) and data (right). The MC plot shows the expected signal peak and background contributions from  $\Xi^0 \rightarrow \Lambda\pi^0$  and  $\Sigma^{*0} \rightarrow \Lambda\pi^0$  decays with only one reconstructed photon.

## 6 CONCLUSION

We have reported the results of a study of strange particle production in  $\nu_\mu$  CC interactions using the data from the NOMAD experiment. Our analysis is based on a sample of  $\nu_\mu$  CC events containing 15074 identified  $K_s^0$ , 8087 identified  $\Lambda$  and 649 identified  $\bar{\Lambda}$  decays. This  $V^0$  sample represents at least a factor of 5 increase in statistics compared to previous (anti)neutrino experiments performed with bubble chambers. Yields of neutral strange particles ( $K_s^0$ ,  $\Lambda$ ,  $\bar{\Lambda}$ ) have been measured in this analysis as a function of kinematic variables. For  $\bar{\Lambda}$  production such measurements are performed for the first time in a neutrino experiment. The decays of resonances and heavy hyperons with identified  $K_s^0$  and  $\Lambda$  in the final state have been analyzed. Clear signals corresponding to  $K^{*\pm}$ ,  $\Sigma^{*\pm}$ ,  $\Xi^-$  and  $\Sigma^0$  have been observed. This study is potentially interesting for the tuning of Monte Carlo simulation programs and is also of special importance for a quantitative theoretical interpretation of the  $\Lambda$  and  $\bar{\Lambda}$  polarization measurements reported earlier [27, 28].

## Acknowledgements

We gratefully acknowledge the CERN SPS accelerator and beam-line staff for the

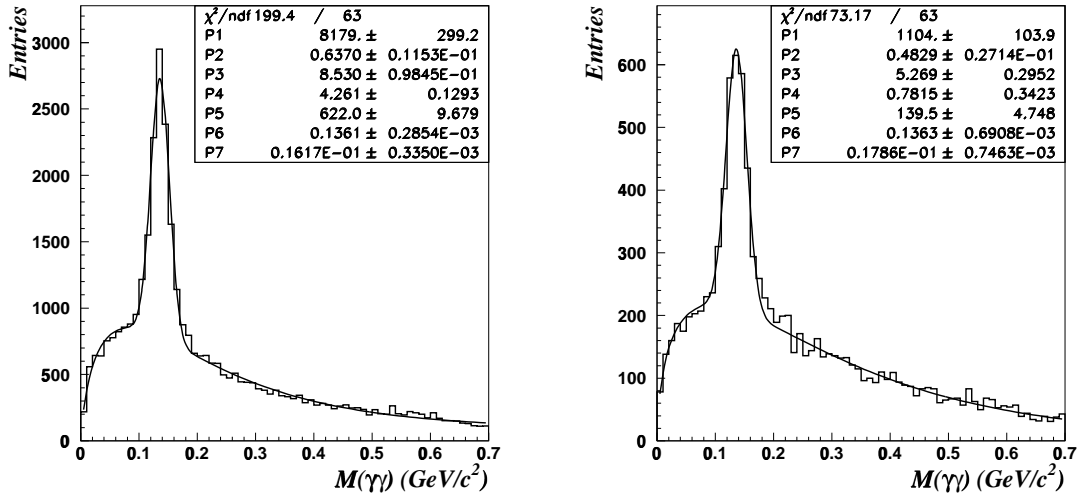


Figure 25:  $\gamma\gamma$  invariant mass distributions for MC (left) and data (right). Both photons have been reconstructed as conversions in the DC fiducial volume and identified by our  $V^0$  identification procedure. A clear peak corresponding to the  $\pi^0$  signal is visible in both distributions. The parameters  $P_6$  and  $P_7$  show the mass and the width of the Gaussian function after the fit.

Table 16:  $\Sigma^0 \rightarrow \Lambda\gamma$  summary

N( $\Sigma^0$ )	full sample	$\Lambda$ fragmentation region		type of target nucleon	
		$x_F < 0$	$x_F > 0$	$\nu p$	$\nu n$
DATA	29 ± 10	17 ± 9	16 ± 7	16 ± 7	13 ± 7
MC(meas.)	82 ± 12	50 ± 9	37 ± 8	19 ± 7	61 ± 10
MC(pred.)	80	57	22	22	57
N( $\Sigma^0$ )/N( $\Lambda$ )	uncorrected				
DATA (%)	0.4 ± 0.1	0.3 ± 0.2	0.7 ± 0.3	0.5 ± 0.2	0.3 ± 0.2
MC (%)	0.7 ± 0.1	0.6 ± 0.1	1.2 ± 0.3	0.5 ± 0.2	0.8 ± 0.1

magnificent performance of the neutrino beam. We also thank the technical and secretarial staff of the collaborating institutes. The experiment was supported by the following funding agencies: Australian Research Council (ARC) and Department of Industry, Science, and Resources (DISR), Australia; Institut National de Physique Nucléaire et Physique des Particules (IN2P3), Commissariat à l’Energie Atomique (CEA), France; Bundesministerium für Bildung und Forschung (BMBF, contract 05 6DO52), Germany; Istituto Nazionale di Fisica Nucleare (INFN), Italy; Joint Institute for Nuclear Research and Institute for Nuclear Research of the Russian Academy of Sciences, Russia; Fonds National Suisse de la Recherche Scientifique, Switzerland; Department of Energy, National Science Foundation (grant PHY-9526278), the Sloan and the Cottrell Foundations, USA.

## References

- [1] S.J.Barish *et al.*, Phys. Rev. Lett. **33** (1974) 1446
- [2] H.Deden *et al.*, Phys. Lett. **B58** (1975) 361
- [3] J.P.Berge *et al.*, [E45 Collaboration], Phys. Rev. Lett. **36** (1976) 127

Table 17: Corrected fractions (in %) of observed  $K_s^0$  and  $\Lambda$  decays that originate from the decays of strange resonances and heavy hyperons in the NOMAD data compared to the default MC predictions.

	$K^{*+} \rightarrow K_s^0 \pi^+$	$K^{*-} \rightarrow K_s^0 \pi^-$	$\Sigma^{*+} \rightarrow \Lambda \pi^+$	$\Sigma^{*-} \rightarrow \Lambda \pi^-$	$\Sigma^0 \rightarrow \Lambda \gamma$	$\Xi^- \rightarrow \Lambda \pi^-$
DATA	$15.5 \pm 0.9$	$8.7 \pm 0.7$	$5.8 \pm 1.1$	$2.6 \pm 0.8$	$7.3 \pm 2.4$	$1.9 \pm 1.7$
MC	31.4	13.1	16.6	3.9	12.7	1.5

- [4] H.Deden *et al.*, Phys. Lett. **B67** (1977) 474
- [5] J.P.Berge *et al.*, [E45 Collaboration], Phys. Rev. **D18** (1978) 1359
- [6] O.Erriquez *et al.*, Nucl. Phys. **B140** (1978) 123
- [7] V.V.Ammosov *et al.*, Nucl. Phys. **B162** (1980) 205
- [8] N.J.Baker *et al.*, [E427 Collaboration], Phys. Rev. **D24** (1981) 2779
- [9] V.V.Ammosov *et al.*, Nucl. Phys. **B177** (1981) 365
- [10] R.Brock *et al.*, [E31 Collaboration], Phys. Rev. **D25** (1982) 1753
- [11] H.Grässler *et al.*, Nucl. Phys. **B194** (1982) 1
- [12] P.Bosetti *et al.*, [WA47 Collaboration], Nucl. Phys. **B209** (1982) 29
- [13] D.Son *et al.*, Phys. Rev. Lett. **49** (1982) 1128, **49** (1982) 1800 (erratum)
- [14] D.Allasia *et al.*, [WA25 Collaboration], Nucl. Phys. **B224** (1983) 1
- [15] C.C.Chang *et al.*, Phys. Rev. **D27** (1983) 2776
- [16] D.Son *et al.*, Phys. Rev. **D28** (1983) 2129
- [17] D.Allasia *et al.*, [WA25 Collaboration], Phys. Lett. **B154** (1985) 231
- [18] G.T.Jones *et al.*, [WA21 Collaboration], Z. Phys. **C28** (1985) 23
- [19] N.J.Baker *et al.*, [E380 Collaboration], Phys. Rev. **D34** (1986) 1251
- [20] W.A.Mann *et al.*, Phys. Rev. **D34** (1986) 2545
- [21] V.V.Ammosov *et al.*, [SKAT Collaboration], Z. Phys. **C30** (1986) 183
- [22] V.V.Ammosov *et al.*, Z. Phys. **C36** (1987) 377
- [23] S.Willocq *et al.*, [WA59 Collaboration], Z. Phys. **C53** (1992) 207
- [24] G.T.Jones *et al.*, [WA21 Collaboration], Z. Phys. **C57** (1993) 197
- [25] D.DeProspero *et al.*, [E632 Collaboration], Phys. Rev. **D50** (1994) 6691
- [26] J.Altegoer *et al.*, [NOMAD Collaboration], Nucl. Instr. and Meth. **A404** (1998) 96
- [27] P.Astier *et al.*, [NOMAD Collaboration], Nucl. Phys. **B588** (2000) 3
- [28] P.Astier *et al.*, [NOMAD Collaboration], Nucl. Phys. **B605** (2001) 3
- [29] J.Altegoer *et al.*, [NOMAD Collaboration], Phys. Lett. **B431** (1998) 219  
P.Astier *et al.*, [NOMAD Collaboration], Phys. Lett. **B453** (1999) 169  
P.Astier *et al.*, [NOMAD Collaboration], Phys. Lett. **B483** (2000) 387  
P.Astier *et al.*, [NOMAD Collaboration], Nucl. Phys. **B611** (2001) 3
- [30] G.Ingelman, LEPTO version 6.1, “The Lund Monte Carlo for Deep Inelastic Lepton-Nucleon Scattering”, TSL-ISV-92-0065 (1992)  
G.Ingelman, A.Edin, J.Rathsman, LEPTO version 6.5, Comp. Phys. Comm. **101** (1997) 108, [hep-ph/9605286]
- [31] T.Sjöstrand, “PYTHIA 5.7 and JETSET 7.4: physics and manual”, LU-TP-95-20 (1995), [hep-ph/9508391]  
T.Sjöstrand, Comp. Phys. Comm **39** (1986) 347, **43** (1987) 367
- [32] GEANT : Detector Description and Simulation Tool, *CERN Programming Library Long Writeup W5013*, GEANT version 3.21
- [33] M.Glück, E.Reya, A.Vogt, Z. Phys. **C53** (1992) 127

- [34] H.Plothow-Besch, *Comp. Phys. Comm.* **75** (1993) 396
- [35] P.Astier *et al.*, [NOMAD Collaboration], “Prediction of neutrino fluxes in the NOMAD experiment”, *paper in preparation*
- [36] M.Anfreville *et al.*, “The drift chambers of the NOMAD experiment”, hep-ex/0104012, *to be published in Nucl. Instr. and Meth.*
- [37] G.Bassompierre *et al.*, *Nucl. Instr. and Meth.* **A403** (1998) 363;  
G.Bassompierre *et al.*, *Nucl. Instr. and Meth.* **A411** (1998) 63
- [38] D.Autiero *et al.*, *Nucl. Instr. and Meth.* **A373** (1996) 358;  
D.Autiero *et al.*, *Nucl. Instr. and Meth.* **A387** (1997) 352;  
D.Autiero *et al.*, *Nucl. Instr. and Meth.* **A411** (1998) 285
- [39] D.V.Naumov, PhD Thesis, JINR, Dubna, Russia, 2001, *in Russian*
- [40] Review of Particle Properties, *Eur. Phys. J.* **C15** (2000)
- [41] G.T.Jones *et al.*, [WA21 Collaboration], *Z. Phys.* **C27** (1985) 43
- [42] P.D.Acton *et al.*, [OPAL Collaboration], *Z. Phys.* **C56** (1992) 521
- [43] P.Abreu *et al.*, [DELPHI Collaboration], *Z. Phys.* **C65** (1995) 587
- [44] M.R.Adams *et al.*, [E665 Collaboration], *Z. Phys.* **C61** (1994) 539
- [45] M.Derrick *et al.*, [ZEUS Collaboration], *Z. Phys.* **C68** (1995) 29
- [46] S.Aid *et al.*, [H1 Collaboration], *Nucl. Phys.* **B480** (1996) 3
- [47] P.C.Bosetti *et al.*, [WA21 & WA47 Collaboration], *Z. Phys.* **C46** (1990) 377  
G.T.Jones *et al.*, [WA21 Collaboration], *Z. Phys.* **C25** (1984) 121
- [48] C.Lachaud, PhD Thesis, Université Denis Diderot (Paris 7), May 2000, *in French*
- [49] J.D.Jackson, *Nuovo Cimento* **34** (1964) 1644
- [50] MINUIT package, *CERN Program Library Long Writeup* **D506** (1994)